Astronomy & Astrophysics manuscript no. paper
May 13, 2014

The Wolf-Rayet stars in the Large Magellanic Cloud⋆

A comprehensive analysis of the WN class

R. Hainich[1], U. Rühling[1], H. Todt[1], L. M. Oskinova[1], A. Liermann[2], G. Gräfener[3], C. Foellmi[4], O. Schnurr[2], and W.-R. Hamann[1]

[1] Institut für Physik und Astronomie, Universität Potsdam, Karl-Liebknecht-Str. 24/25, D-14476 Potsdam, Germany
e-mail: rhainich@astro.physik.uni-potsdam.de
[2] Leibniz-Institut für Astrophysik Potsdam, An der Sternwarte 16, D-14482 Potsdam, Germany
[3] Armagh Observatory, College Hill, Armagh BT6 9D, UK
[4] 12 rue Servan, 38000 Grenoble, France

Received <date> / Accepted <date>

ABSTRACT

Context. Massive stars, although being important building blocks of galaxies, are still not fully understood. This especially holds true for Wolf-Rayet (WR) stars with their strong mass loss, whose spectral analysis requires adequate model atmospheres.
Aims. Following our comprehensive studies of the WR stars in the Milky Way, we now present spectroscopic analyses of almost all known WN stars in the LMC.
Methods. For the quantitative analysis of the wind-dominated emission-line spectra, we employ the Potsdam Wolf-Rayet (PoWR) model atmosphere code. By fitting synthetic spectra to the observed spectral energy distribution and the available spectra (ultraviolet and optical), we obtain the physical properties of 107 stars.
Results. We present the fundamental stellar and wind parameters for an almost complete sample of WN stars in the LMC. Among those stars that are putatively single, two different groups can be clearly distinguished. While 12 % of our sample are more luminous than $10^6\,L_\odot$ and contain a significant amount of hydrogen, 88 % of the WN stars, with little or no hydrogen, populate the luminosity range between $\log(L/L_\odot) = 5.3 \ldots 5.8$.
Conclusions. While the few extremely luminous stars ($\log(L/L_\odot) > 6$), if indeed single stars, descended directly from the main sequence at very high initial masses, the bulk of WN stars have gone through the red-supergiant phase. According to their luminosities in the range of $\log(L/L_\odot) = 5.3 \ldots 5.8$, these stars originate from initial masses between 20 and 40 $M_\odot$. This mass range is similar to the one found in the Galaxy, i.e. the expected metallicity dependence of the evolution is not seen. Current stellar evolution tracks, even when accounting for rotationally induced mixing, still partly fail to reproduce the observed ranges of luminosities and initial masses. Moreover, stellar radii are generally larger and effective temperatures correspondingly lower than predicted from stellar evolution models, probably due to subphotospheric inflation.

Key words. Stars: Wolf-Rayet – Magellanic Clouds – Stars: early type – Stars: atmospheres – Stars: winds, outflows – Stars: mass-loss

1. Introduction

The Large Magellanic Cloud (LMC) is one of the closest galaxies to the Milky Way (MW), allowing detailed spectroscopy of its brighter stars. Its distance modulus of only $DM = 18.5$ mag is well constrained (Madore & Freedman 1998; Pietrzyński et al. 2013). Another advantage in analyzing stars of the LMC is the marginal reddening along the line of sight (Subramaniam 2005; Haschke et al. 2011), which is in general below $E_{b-v} = 0.25$ mag (Larsen et al. 2000).

Compared to our Galaxy, the LMC is much smaller and has a deviating structure that is intermediate between a dwarf spiral and an irregular type. The LMC exhibits a very different history of star formation than the MW. The metallicity observed in LMC stars is, in general, subsolar ($Z/Z_\odot \sim 0.4$, Dufour et al. 1982), but with a strong age-dependence (e.g., Piatti & Geisler 2013). For young massive stars, it may reach nearly solar values. In the stellar evolution calculations that we will discuss below, Meynet & Maeder (2005) adopted $Z = 0.008$, which is about 60 % of the solar value (Asplund et al. 2009).

The metallicity is expected to have significant influence on the evolution of massive stars as it has impact on the mass loss due to stellar winds. As far as these winds are driven by radiation pressure on spectral lines of metals like iron, the mass-loss rate is expected to scale with Z^m with $m \approx 0.5$ (e.g., Kudritzki et al. 1989). Based on their theoretical models, Vink & de Koter (2005) derived an exponent of $m = 0.86$ for late-type Wolf-Rayet (WR) stars. The fact that the distribution of the WR stars on the subclasses (i.e., the nitrogen sequence: WN and the carbon sequence: WC) strongly differs between the LMC and the MW is generally attributed to this metallicity effect. Eldridge & Vink (2006) found that the mass-loss rates from Vink & de Koter (2005) can account for the observed WC/WN ratio as a function of the metallicity. The metallicity dependence of the WN

⋆ Partly based on observations made with the NASA/ESA Hubble Space Telescope, and obtained from the Hubble Legacy Archive, which is a collaboration between the Space Telescope Science Institute (STScI/NASA), the Space Telescope European Coordinating Facility (ST-ECF/ESA), and the Canadian Astronomy Data Centre (CADC/NRC/CSA).

mass-loss was affirmed by the hydrodynamic stellar wind models presented by Gräfener & Hamann (2008).

In previous papers, we have concentrated on analyzing the WR population of the MW. In Hamann et al. (2006, hereafter HGL06), we presented a comprehensive analysis of the Galactic WN stars, while the WC subtypes were studied by Sander et al. (2012). For both classes we found discrepancies between the parameters of the observed WR population and the predictions of the available stellar evolution calculations.

The current paper focuses on the WR stars in the LMC. With more than 100 objects, our sample comprise nearly all WN-type stars known in the LMC. In contrast, earlier analyses of WN stars in the LMC were limited to a sample size below 20 objects (Crowther & Smith 1997; Crowther & Dessart 1998; Hamann & Koesterke 2000) and were often confined to specific subclasses (Crowther et al. 1995a; Pasquali et al. 1997).

At the time of these studies, stellar atmosphere models commonly did not yet account for iron-line blanketing (Hillier & Miller 1999; Gräfener et al. 2002) and wind inhomogeneities. The inclusion of these two effects, the latter by means of the microclumping approach (cf. Hamann & Koesterke 1998), significantly improved stellar atmosphere models and entailed a pervasive revision of the derived stellar parameters (e.g., Hamann & Koesterke 2000; Crowther et al. 2002, 2010; Sander et al. 2012). Similar profound improvements were achieved in the field of stellar evolution by the inclusion of physical processes such as stellar rotation (Meynet & Maeder 2003, 2005) and, more recently, magnetic fields (Maeder & Meynet 2005; Yoon et al. 2012).

In the last decade, high signal to noise spectra in the optical spectral range of almost all WN stars in the LMC were obtained in extensive spectroscopic studies realized by Foellmi et al. (2003b) and Schnurr et al. (2008). For the first time, the spectra obtained by these two studies make it possible to analyze a comprehensive sample of LMC WN stars. By this means, we obtain a general overview of a nearly complete WN-star population, which we employ to test state-of-the-art evolution models.

This paper is organized as follows: In the next Section, we introduce our sample of stars and the observational data employed. In Sect. 3, we briefly characterize the Potsdam Wolf-Rayet (PoWR) model atmospheres. The method of our analyses is described in Sect. 4. The results are compiled in Sect. 5. In Sect. 6, we discuss our results with respect to the stellar evolution theory. A summary and conclusions are presented in Sect. 7.

The *Online Material* gives details about the observational data (Appendix A) and comments on the individual stars (Appendix B). Finally, we provide spectral fits for all sample stars (Appendix C).

2. The sample

2.1. Sample selection

Our sample is based on the fourth catalog of WR stars in the LMC (Breysacher et al. 1999, hereafter BAT99). Throughout this paper, we identify the stars by their running number in that list. In this catalog, a spectral type of the WN sequence was assigned to each of the 109 objects.

In a few cases, the spectral classification had to be revised. The stars BAT99 45 and BAT99 83 are actually luminous blue variables (LBVs) (see Humphreys & Davidson 1994; Schnurr et al. 2008) and are, therefore, excluded from our sample.

Five of the stars listed with a WN classification in the BAT99 catalog have been reclassified as Of-types: BAT99 107 has been identified as a massive spectroscopic binary system comprising two Of-type stars (Taylor et al. 2011). Niemela et al. (2001) found BAT99 6 to be an O-type binary system as well. Crowther & Walborn (2011) have reclassified BAT99 105 and BAT99 110 as O2If* stars. The spectral type O3If* has been assigned to BAT99 93 by Evans et al. (2011). Despite their reclassifications, we keep these O-type objects in our sample. Thus, the number of proper WN stars from the original BAT99 catalog is reduced to 102.

Since the publication of the BAT99 catalog, only a few additional WN stars have been identified in the LMC. A list of the seven newly discovered WR stars, six of them WN-type stars, can be found in Table 3 of Neugent et al. (2012). Thus, the number of known WN stars in the LMC amounts to 108, although two of these new detections are precarious. Massey et al. (2000) identified Sk -69° 194 as B0 Ia + WN. However, Foellmi et al. (2003b) could not confirm this detection. Neugent et al. (2012) also list LH 90β-6 as a new WN star. However, according to Massey et al. (2000), this is an alias of TSWR 1, which was resolved into multiple components by Walborn et al. (1999) and incorporated in the BAT99 catalog with the number BAT99 78. Therefore, the basis of this new detection is not clear. Another six new WR stars in the LMC are reported by Reid & Parker (2012), but without giving coordinates or closer classifications. We do not include any of these newly discovered WN stars in our analyses.

With 102 out of 108 known WN stars in the LMC, our sample covers this class nearly completely with all subtypes present. The spatial distribution of our program stars is illustrated in Fig. 1, and the complete list of analyzed objects (including the five Of stars) is compiled in Table 2. For the majority of our sample, the spectral types have been determined by Foellmi et al. (2003b) and Schnurr et al. (2008), respectively, based on the classification scheme elaborated by Smith et al. (1996). For the handful of stars missing in their samples, we adopt the spectral type from the BAT99 catalog. A couple of our stars have been reclassified by various authors since the publication of these catalogs. The present classification of each star is quoted in Table 2. The subtypes WN2 to WN5 are sometimes referred to as WNE ("early"), while WN6 to WN11 are referred to as WNL ("late").

The total census of WR stars in the LMC, as far as they are assigned to their subclass, amounts to 134. In addition to the 108 WN stars, only 24 WC stars plus two WR stars with prominent oxygen lines (WO stars) were discovered (Barlow & Hummer 1982; Neugent et al. 2012). The composition of the WR population is thus very different from our Galaxy, where the ratio of WN to WC stars is close to unity.

2.2. Binaries

Among the objects in our sample some may be binary (or multiple) systems. We, therefore, carefully consider the binary status of each object. All stars for which Foellmi et al. (2003b), Schnurr et al. (2008), or BAT99 list periodic radial-velocity variations are considered as confirmed binaries (cf. Table 2).

For some of our targets there are less conclusive radial-velocity measurements or binary classifications based on spectral peculiarities. Such cases are considered binary suspects, as indicated by a question mark in Table 2 with the corresponding references.

Another method to identify WR stars as binaries is to evaluate their X-ray luminosity. According to studies of Galactic WR-stars, single WC-type stars are not X-ray sources at all (Oskinova et al. 2003), while single WN-type stars in general are rel-

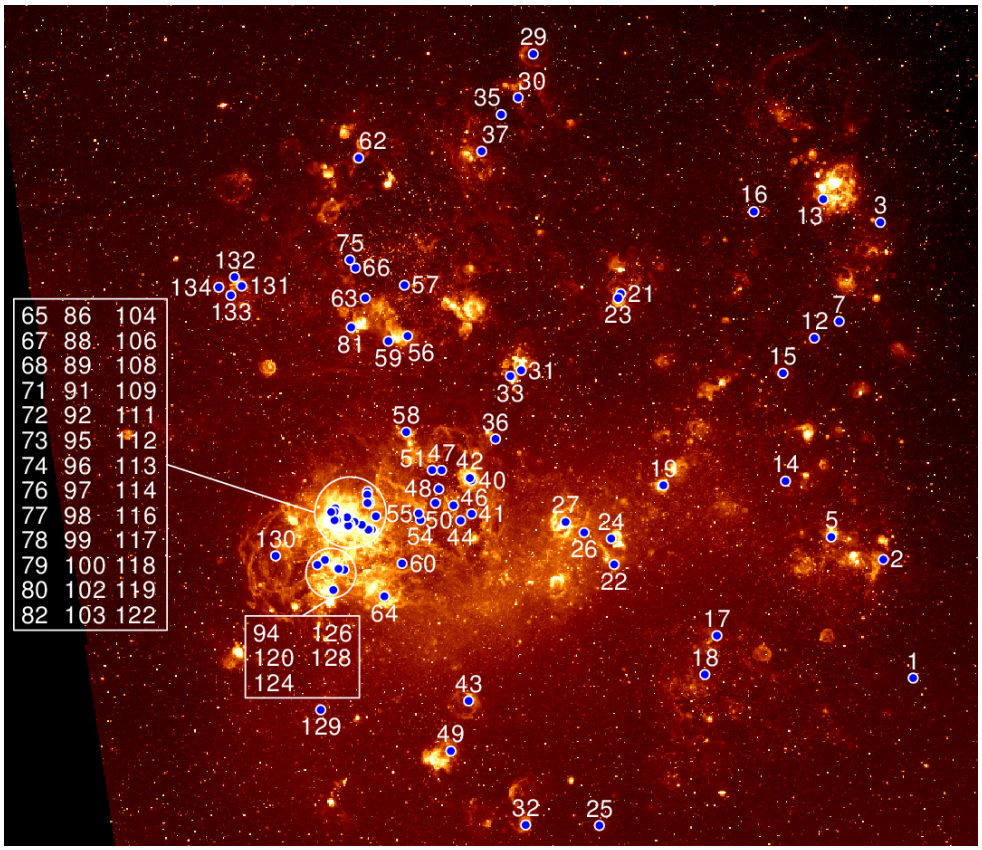

Fig. 1. The WN stars of our sample, identified by their number in the BAT99 catalog. The two boxes refer to the very crowded region of 30 Doradus. The Hα image in the background is from the Magellanic Cloud Emission-Line Survey (MCELS, Smith et al. 2005).

atively X-ray faint. Some of them remain undetected in X-rays despite quite sensitive observations, setting strict upper limits on the X-ray luminosity. For example, Gosset et al. (2005) obtained $L_X < 2 \times 10^{30}$ erg s^{-1} for WR 40 (WN8). The X-ray luminosities of those WN stars that were detected are relatively small, not exceeding a few times 10^{32} erg s^{-1} (Ignace et al. 2000, 2003; Skinner et al. 2012). The mechanism of X-ray production in single WN stars is not fully understood, but is thought to be related to the presence of clumps and large scale structures in their winds (Chené et al. 2011; Oskinova et al. 2012).

In contrast, binary WR stars with colliding winds are significantly more X-ray luminous than single stars. In such systems, the production of X-rays is explained by the heating of gas in a strong shock that results when two stellar winds collide (Stevens et al. 1992). Therefore, a higher than usual X-ray luminosity can serve as a good indicator for a colliding wind binary. As an example, the high X-ray luminosity of the Galactic star WR 25 ($L_X = 1.3 \times 10^{34}$ erg s^{-1}) provided strong indications that this star is a colliding-wind binary (Raassen et al. 2003), as confirmed later from radial velocity measurements (Gamen et al. 2006).

Binary WR-stars with a compact companion, i.e., with a neutron star or black hole, are expected to have even higher X-ray luminosities exceeding 10^{35} erg s^{-1}. The X-ray luminosities in these systems are powered by the wind accretion onto the companion. An intriguing example is Cyg X-3, a Galactic high-mass X-ray binary with a WN-type primary, which has an X-ray luminosity of 10^{38} erg s^{-1} (e.g., Lommen et al. 2005).

The X-ray properties of WR stars in the Magellanic Clouds were studied systematically by Guerrero & Chu (2008a,b), using observations with the X-ray observatories *Rosat* and *Chandra*. The sensitivity of these surveys was limited to X-ray luminosities of a few times 10^{32} erg s^{-1}. They detected X-rays from 27 of the WR stars in the LMC, with X-ray luminosities being similar to those of Galactic colliding-wind binaries. Since there is no reason to assume that single WR-stars in the LMC are intrinsically more bright in X-rays than in the Galaxy, we suspect all WR stars detected by Guerrero & Chu to be colliding wind binaries and mark them accordingly in Table 2.

Altogether, our sample (without the Of stars) includes 17 confirmed binaries plus 22 binary suspects. From 108 known WN stars in the LMC, this corresponds to a binary frequency of only 16 – 36 %. Although this binary fraction seems to be a bit low, it is in line with expectations from binary population studies (e.g., Foellmi et al. 2003a; Chini et al. 2012; Sana et al. 2012, 2013a). Moreover, there are most likely more binaries in our sample that are not yet recognized.

2.3. Observational data

This study was facilitated by optical spectra obtained by Foellmi et al. (2003b) who observed 61 WNE stars with various instruments between 1998 and 2002. These data are publicly available[1]. The completeness of this study was only possible due to spectroscopic observations of 42 late-type WN stars carried out by Schnurr et al. (2008). For details on the instrumentation and data reduction, we refer to Foellmi et al. (2003b) and Schnurr et al. (2008). These two sets of data were primarily designed to search for radial velocity variations, the results being published

[1] `http://wikimbad.obs.ujf-grenoble.fr/Category_Wolf-Rayet_Star.html`

in Foellmi et al. (2003b) and Schnurr et al. (2008). These spectra were not flux-calibrated and have been normalized by the respective authors.

From the VizieR archive we retrieved flux-calibrated, low-resolution optical spectra for most of our targets, recorded by Torres-Dodgen & Massey (1988) on a SIT-vidicon detector at the Cassegrain spectrograph of the 1.5 m telescope of the Cerro Tololo Inter-American Observatory (CTIO). Furthermore, we reused 19 observations dating back to 1989 (cf. Koesterke et al. 1991), obtained with the the ESO Faint Object Spectrograph and Camera (EFOSC) at the 3.6 m telescope. Unreduced spectra of WN and Of stars observed with the Anglo-Australian Telescope (AAT) were obtained from the study by Crowther & Smith (1997). We performed the wavelength calibration with given arc lamp data and normalized them "by eye" if no other optical spectra were at hand.

Ultraviolet spectra secured with the International Ultraviolet Explorer (IUE) are available from the archives for almost all of the stars of our sample, except for those located in the very crowded 30 Dor region. Especially for some of the latter, UV and optical spectra were recorded with spectrographs aboard the *Hubble Space Telescope* (HST). A subset of 19 stars have been observed with the Far Ultraviolet Spectroscopic Explorer (FUSE), but these data were not used in the current study. The FUSE spectra will be the subject of a detailed abundance analysis of LMC WN stars in a subsequent paper.

Before fitting the observed spectra, we corrected the wavelengths for the radial velocities of the individual stars, mostly taken from Foellmi et al. (2003b) and Schnurr et al. (2008). The details about the origin of all spectra employed in this paper are compiled in Table A.1 in the *Online Material*.

We used narrowband optical photometry (u, b, v) obtained by Crowther & Hadfield (2006) whenever available. Otherwise, we used the older measurements from Torres-Dodgen & Massey (1988), and finally complemented the data with values from BAT99. Near-infrared magnitudes (J, H, K_S) were retrieved from the 2MASS catalog (Skrutskie et al. 2006), except for those stars located in the crowded field of 30 Dor. Photometry from the InfraRed Array Camera (IRAC, 3.6, 4.5, 5.8, and 8.0 μm) of the *Spitzer Space Telescope* is available for most stars from the catalog by Bonanos et al. (2009).

3. The models

Our spectral analyses are based on non-local thermodynamic equilibrium (non-LTE) model atmospheres calculated with the PoWR code. Its basic assumptions are spherical symmetry and stationarity of the flow. The radiative transfer equation is solved in the comoving frame, iteratively with the equations of statistical equilibrium and radiative equilibrium. For more details of the PoWR code, see Hamann & Gräfener (2004).

The main parameters of a model atmosphere are the luminosity L and the "stellar temperature" T_*. The latter is the effective temperature related to the stellar radius R_* via the Stefan-Boltzmann law

$$L = 4\pi\sigma R_*^2 T_*^4 \ . \tag{1}$$

The stellar radius R_* is per definition located at a radial Rosseland optical depth of 20, which represents the lower boundary of the model atmosphere.

Additional parameters, which describe the stellar wind, can be combined in the so-called transformed radius R_t. This quantity was introduced by Schmutz et al. (1989); we define it as

$$R_\mathrm{t} = R_* \left(\frac{v_\infty}{2500\,\mathrm{km\,s^{-1}}} \Big/ \frac{\dot{M}\sqrt{D}}{10^{-4}\,M_\odot\,\mathrm{yr}^{-1}} \right)^{2/3} \tag{2}$$

with v_∞ denoting the terminal wind velocity, $\dot{M}$ the mass-loss rate, and D the clumping contrast (see below). Schmutz et al. (1989) noticed that model spectra with equal R_t exhibit approximately the same emission line strengths, independent of the specific combination of the particular wind parameters as long as T_* and the chemical composition are the same. Even the line profile is conserved under the additional condition that v_∞ is also kept constant. One can understand this invariance when realizing that R_t is related to the ratio between the volume emission measure and the stellar surface area.

According to this scaling invariance, a model can be scaled to a different luminosity as long as R_t and T_* are unchanged. Equation (2) implies that the mass-loss rate then must be scaled proportional to $L^{3/4}$ in order to preserve the normalized line spectrum.

Allowing for wind inhomogeneities, the "density contrast" D is the factor by which the density in the clumps is enhanced compared to a homogeneous wind of the same $\dot{M}$. We account for wind clumping in the approximation of optically thin structures (Hillier 1991; Hamann & Koesterke 1998). From the analysis of the electron-scattering line wings in Galactic WN stars, Hamann & Koesterke (1998) found that a density contrast of $D = 4$ is adequate. To the contrary, Crowther et al. (2010) and Doran et al. (2013) inferred $D = 10$ in their analyses of WN stars in the 30 Doradus region. For the current study, we uniformly adopt a density contrast of $D = 10$, because we noticed in a detailed investigation of a subsample that with $D = 4$, the line-scattering wings in the models are stronger than observed. Note that the empirical mass-loss rates derived in this work scale with $D^{-1/2}$ (cf. Eq. 2).

For the Doppler velocity v_D, describing the line broadening due to microturbulence and thermal motion, we adopt a value of $100\,\mathrm{km\,s^{-1}}$, which provides a good fit to the data and is approved in previous studies (e.g., Hamann & Koesterke 2000, hereafter HK2000; HGL06).

For the velocity law $v(r)$ in the supersonic part of the wind, we adopt the so-called β-law. For the exponent β, the radiation-driven wind theory predicts about 0.8 in agreement with observations (e.g., Pauldrach et al. 1986). In WN stars, the law is more shallow because of multiple-scattering effects. We adopt $\beta = 1$, which better resembles the hydrodynamic prediction (Gräfener & Hamann 2007), and yields consistent spectral fits. In the subsonic part, the velocity field is implied by the hydrostatic density stratification according to the continuity equation.

The models are calculated using complex atomic data of H, He, C, and N. Iron group elements are considered in the "superlevel approach" that encompasses $\sim 10^7$ line transitions between $\sim 10^5$ levels within 72 superlevels (Gräfener et al. 2002).

4. Method

To facilitate the analysis of a large number of WN stars, we first establish grids of models. As explained above, the main parameters are the stellar temperature T_* and the transformed radius R_t.

Table 1. Chemical composition (mass fractions in percent)

	Sun[a]	Gal.	LMC			
		WN[b]	B stars[c]	B stars[d]	H II[e]	WN[f]
C	0.237	0.01	0.054	0.086	0.058	0.0067
N	0.069	1.5	0.0083	0.011	0.0087	0.40
O	0.573	-	0.27	0.30	0.281	-
ΣCNO	0.88	1.5	0.33	0.40	0.35	0.41
Fe	0.129	0.14[g]	0.07[h]	-	-	0.07[g]

Notes. [(a)] Asplund et al. (2009) [(b)] as used in HGL06 [(c)] Hunter et al. (2007) [(d)] Korn et al. (2005) [(e)] H II regions (Kurt & Dufour 1998) [(f)] as adopted in this work [(g)] including the whole iron group [(h)] mean value from Trundle et al. (2007)

4.1. Abundances

We calculated three grids of models for different hydrogen abundances: one hydrogen-free "WNE" grid and two "WNL" grids with hydrogen mass fractions of 0.2 and 0.4, respectively. From the trace elements, we account for carbon, nitrogen, and a generic model atom representing the iron-group elements in relative solar mixture (Gräfener et al. 2002).

The material in the WN atmosphere has undergone at least partial CNO burning due to mixing processes in the stellar interior, such as rotational induced mixing (e.g., Heger & Langer 2000). Accordingly, most of the oxygen and carbon was transformed into nitrogen. Assuming equilibrium, the remaining mass fractions of oxygen and carbon relative to that of nitrogen should be only 1/60 (Schaerer et al. 1993). Hence, the nitrogen abundance should roughly equal the sum of the C, N, and O abundances of the initial material from which the star was formed. Note that HK2000 inferred a nitrogen abundance for the Galactic WN stars nearly twice the sum of solar CNO (cf. Table 1).

As a reference for LMC abundances, we use spectral analyses of B-type stars. The results from two such studies (Hunter et al. 2007; Korn et al. 2005) are listed in Table 1. Moreover, the table gives abundances found in H II regions of the LMC (Kurt & Dufour 1998). Compared to solar abundances, the sum of C, N, and O in these LMC objects is roughly half the solar value. We, therefore, adopt a nitrogen mass fraction of 0.004 for the models throughout this paper. The carbon abundance is set to 1/60 of this value. We neglect oxygen in our WN star models, since no prominent O lines are present in the optical wavelength range, nor do we expect it to influence the atmospheric stratification.

The iron abundance in B-type stars from several clusters in the LMC has been studied by Trundle et al. (2007) (see Table 1). On average, this value is 0.0007 (mass fraction), i.e., again roughly half the solar iron abundance. We adopted this value as the iron-group abundance for our LMC models.

A detailed abundance analysis is beyond the scope of the present paper. However, the spectral fits presented below reveal that the models cannot reproduce the observed nitrogen lines for a subset of our sample. Thus, it seems that the N abundance in these LMC WN stars is slightly higher than our adopted value.

4.2. The model grids

Three large grids of WN models were computed. The parameter domain of each grid is spanned by T_* and R_t. The grid spacing is 0.05 dex in $\log(T_*/\mathrm{kK})$ and 0.1 dex in $\log(R_t/R_\odot)$ (see Hamann & Gräfener 2004, for details). The luminosity is fixed at $\log(L/L_\odot) = 5.3$. Thanks to the scaling invariance described in Sect. 3, the normalized line spectra apply in good approximation to different luminosities, while the absolute fluxes scale with L.

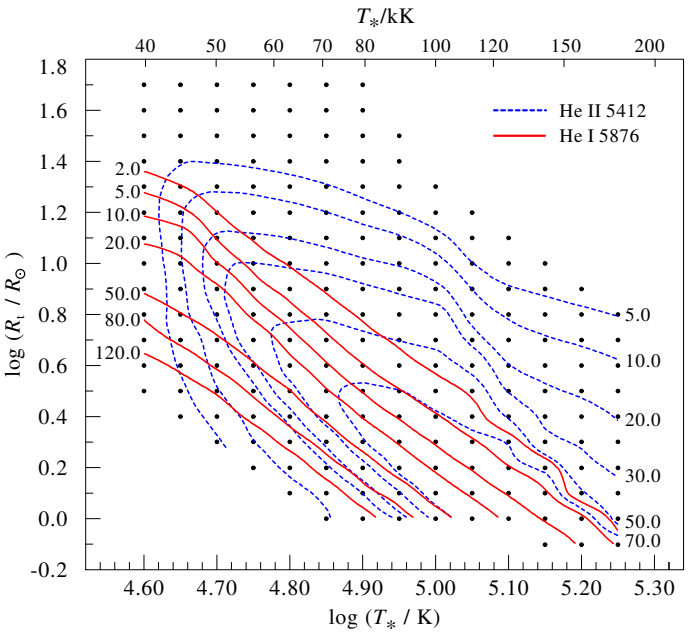

Fig. 2. Grid of models for hydrogen-free WN stars in the LMC: contours of constant line emission, labeled with the equivalent width in Å; thick (red) contours: He I line at 5876 Å, thin-dashed (blue) contours: He II at 5412 Å. Tiny dots indicate calculated grid models.

The three grids differ not only in the hydrogen mass fraction (0, 0.2, and 0.4, respectively), but also in the terminal wind velocity. One grid has been computed for WNE stars with $X_H = 0$ and $v_\infty = 1600\,\mathrm{km\,s^{-1}}$. The other two grids were established for WNL stars ($X_H = 0.2$ and $X_H = 0.4$), respectively, with $v_\infty = 1000\,\mathrm{km\,s^{-1}}$ in both cases. The trace element abundances are set to the values described in Sect. 4.1. These model grids are publicly available on our website[2].

Analyzing a star thus means to identify the specific model which gives the best fit to the observations. A first orientation can be obtained from contour plots like the one shown in Fig. 2. If, for example, the He II emission line at 5412 Å is observed with an equivalent width of 30 Å, the temperature is restricted to values above 50 kK. Combining this with the measured equivalent width of the He I line at 5876 Å, preliminary model parameters can already be estimated from the intersection point of the corresponding contours.

This method works, of course, only if the He I and the He II lines are both present in the spectrum of the considered star. For those stars where this is not the case, such as very hot stars, other ions or elements must be employed. These contour plots are provided on the PoWR homepage for several transitions of the ions He I, He II, N III, N IV, and N V. As is evident from Fig. 2, the method may also fail in the lowest part of the diagram, i.e., for the densest winds, because the contours do not intersect in this parameter regime. At these parameters, the winds are so thick that the whole spectrum, including the continuum, is formed in the rapidly moving part of the wind. For a fixed luminosity, such models have only the mass-loss rate as significant parameter, while the stellar radius and the related effective temperature become meaningless. Due to the spacing chosen for our grid, models of the same mass-loss rate lie on a diagonal of the grid

[2] http://www.astro.physik.uni-potsdam.de/PoWR.html

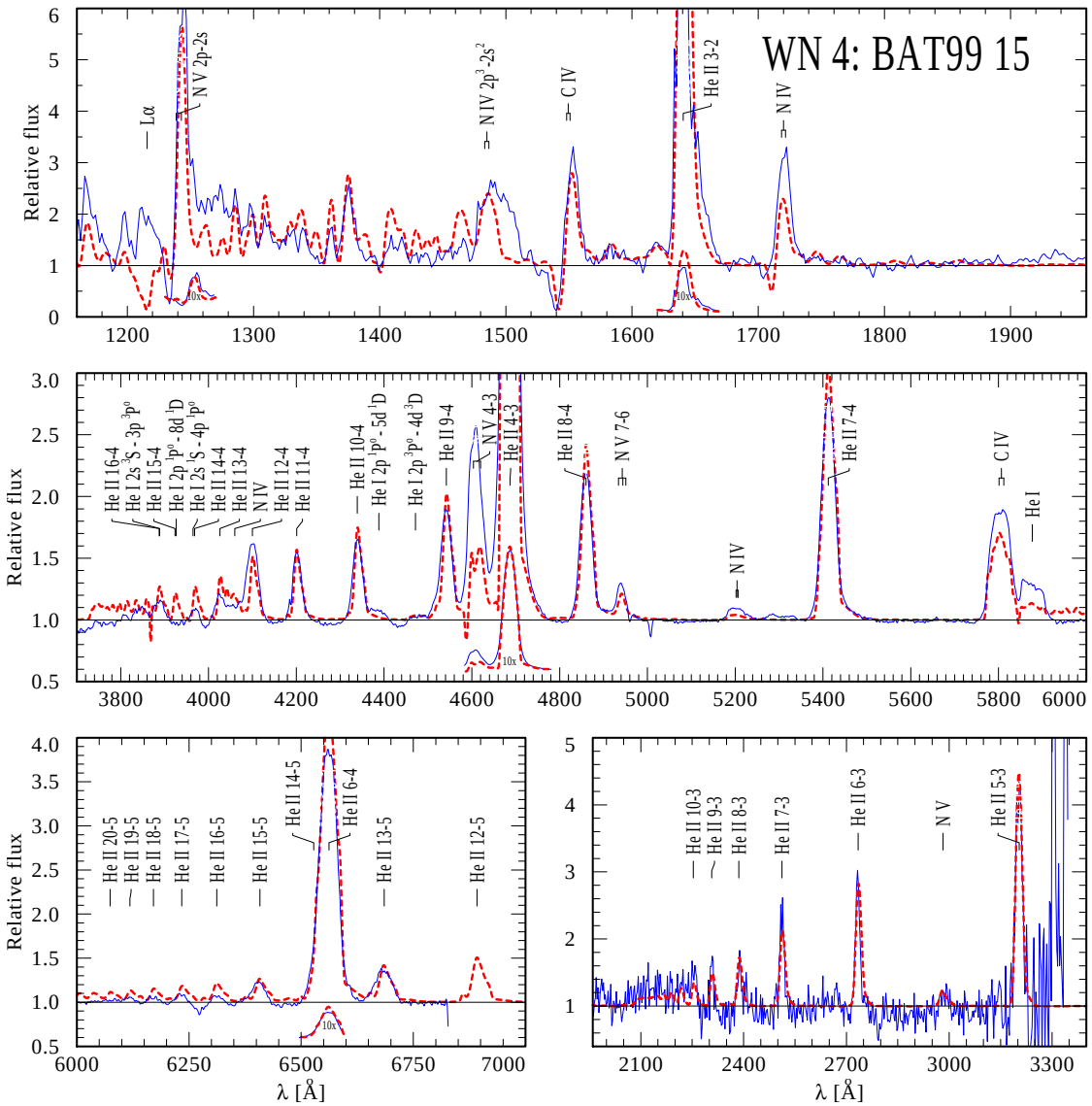

Fig. 3. Normalized spectrum of the WNE star BAT99 015. The thin (blue) solid line depicts the observation, whereas the thick (red) dashed line represents the synthetic spectrum of the best fitting PoWR model.

cells, like the parallel contours. Along these diagonals, the models exhibit fairly similar line spectra. Thus, the stellar parameters derived for stars in the regime of parameter degeneracy solely depend on small differences of the synthetic spectra. There are indeed some stars in our sample that fall into this regime of parameter degeneracy (see Appendix B).

For 27 stars, we preselect suitable grid models by means of a χ^2_ν-fitting technique. This method is based on a reduced χ^2_ν-statistic, which is calculated for the rectified observations with respect to the model spectra in our grids. For details of this fitting technique, we refer to Todt et al. (2013).

4.3. Spectral fitting

After preliminary parameters have been estimated either by the χ^2_ν-fit or by the contour plots, we compare observations and models in detail for each star. A typical fit of the normalized line spectrum is shown in Fig. 3, while analogous plots for each star of the sample can be found in the *Online Material*.

While most of the observed spectra are given in normalized form, some of the spectra (from IUE, HST, and Torres-Dodgen & Massey 1988) are flux-calibrated. These data are normalized consistently through division by the reddened model continuum. In this respect, spectral fitting is an iterative process, coupled with the fitting of the spectral energy distribution described below.

With the starting estimates for T_* and R_t, we carefully compare the observed line spectrum with models of neighboring parameters, and finally determine the best fitting values. The uncertainty is usually smaller than one grid cell, i.e., the error margins are smaller than ±0.05 dex in T_* and ±0.1 dex in R_t. The latter translates to an uncertainty of ±0.15 dex for the mass-loss rate (cf. Eq. 2). This, of course, does not account for systematic errors, because, for instance the model assumptions are not exactly fulfilled.

The terminal wind velocity, v_∞, mainly influences the width of the line profiles. For 62 of our program stars, Niedzielski & Skorzynski (2002) and Niedzielski et al. (2004) measured the wind velocities from P-Cygni profiles in the UV. Depending on the considered line, they obtain quite different values for the same star. Two possible reasons are: (a) While the β-law for the velocity field quickly approaches the terminal velocity, the winds

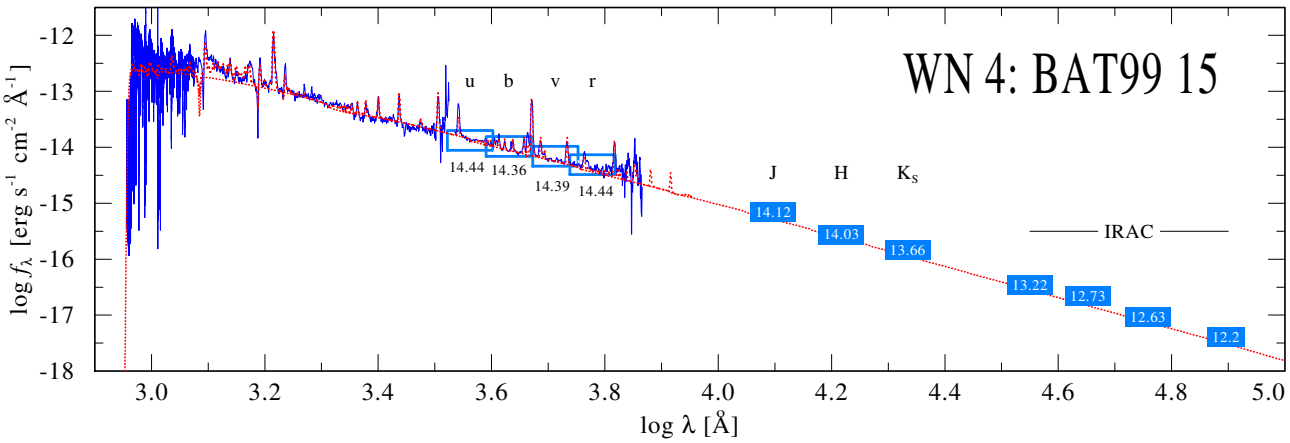

Fig. 4. Spectral energy distribution of the WNE star BAT99 015. Flux-calibrated FUSE, IUE, and CTIO spectra (blue noisy line) and multiband photometry (blue boxes, labeled with the magnitudes) are compared to the model flux (red dotted lines), accounting for interstellar extinction.

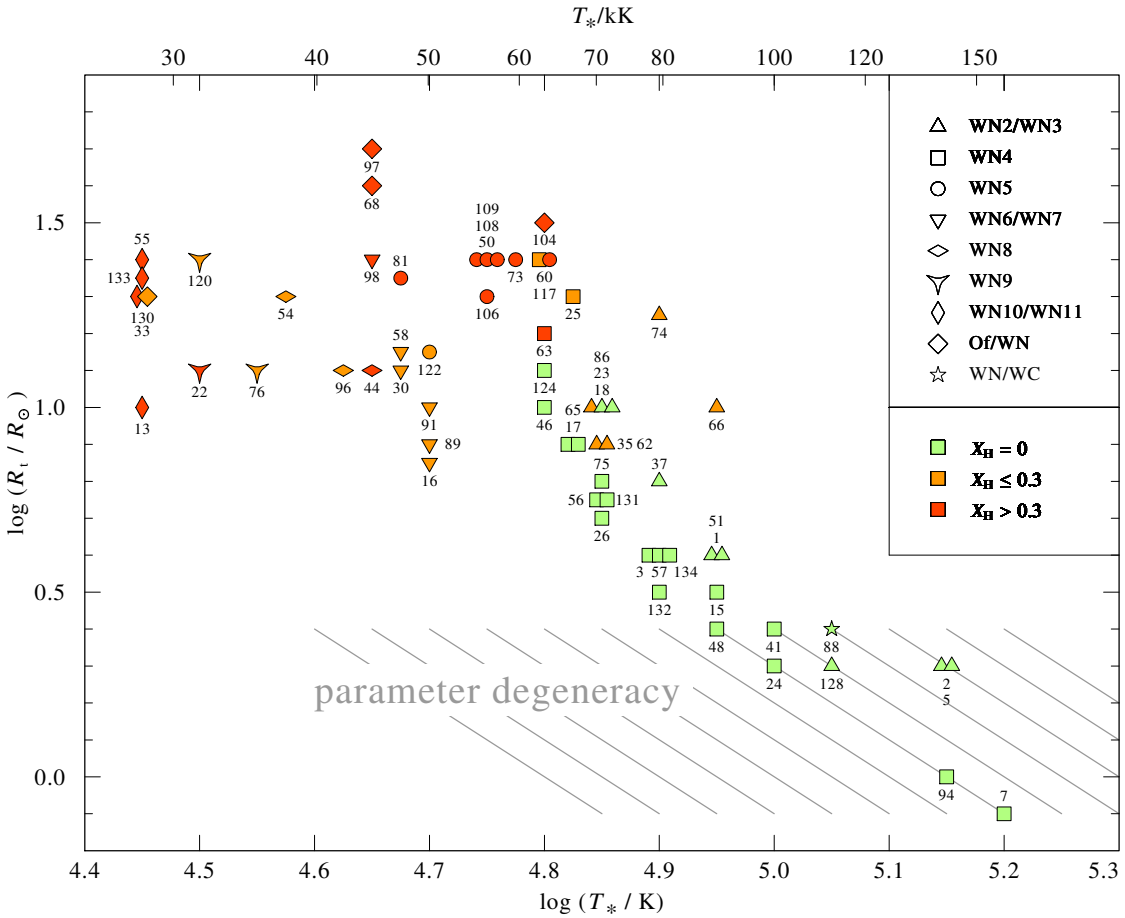

Fig. 5. The positions of the analyzed WN stars in the log T_*-log R_t-plane. The labels refer to the BAT99 catalog. Different WN subtypes are distinguished by the shape of the symbols, as shown in the inlet. The hydrogen abundance is color-coded in three steps (undetectable, about 0.2, and about 0.4 mass fraction). The lower hatched part roughly indicates the region where the parameter space becomes degenerate because of large optical thickness of the wind. In this part, the stars can be shifted parallel to the gray lines without significant changes in the synthetic normalized emission line spectrum.

are in fact further accelerated even at large distances from the star. Therefore, the strongest lines give the highest wind velocity. (b) The velocity field in the wind has some nonuniform, stochastic component that is not perfectly described by our assumption of a constant and isotropic microturbulence. In any case, the largest of the velocities given by Niedzielski et al. (2004) often yield optical emission line profiles that are considerably broader than observed.

Therefore, we prefer to perform our own estimates of v_∞ from the width of the optical emission lines. First, we inspect whether the standard v_∞ of the respective grid is sufficient to reproduce the observed line width. If not, we recalculate the model for the considered star with a more appropriate estimate, aiming at an accuracy of about ±200 km s^{-1}. The values of v_∞ used for the final fits and the subsequent discussion are compiled in Table 2.

Among the studied sample, we found a couple of stars (especially the putatively single WNE stars BAT99 7, 51, 88, and 94) to exhibit very unique spectra. Their emission lines have a round shape that is distinctly different from those of all other stars, but similar to the shape of WR 2 in the Milky Way (HGL06). Such profiles can be reproduced by convolving the model spectrum with a rotation profile of very high $v \sin i$. A more adequate treatment of rotational broadening in WR winds presently confirmed that rotation might in principle account for these spectra (Shenar et al. 2014).

A further important model parameter is the hydrogen abundance. Its determination is one of the major aims of this paper. For this purpose, we calculated three extended model grids for hydrogen mass fractions of 0, 0.2, and 0.4, respectively, plus a couple of models for 0.6. By comparison and tentative interpolation between these grids, we can estimate the hydrogen mass fraction with ±0.1 accuracy.

After the appropriate model has been selected from the line fit, it must be scaled to the correct luminosity by fitting the spectral energy distribution (SED) to the photometric and flux-calibrated observations (for example, see Fig. 4). The scaling corresponds to a simple vertical shift in this logarithmic plot, while the normalized emission line spectrum does not change between models with same transformed radius (cf. Sect. 3). The model flux is geometrically diluted according to the LMC distance modulus of 18.5 mag (Madore & Freedman 1998; Pietrzyński et al. 2013), corresponding to a distance of 50 kpc.

The color excess E_{b-v} must be adjusted simultaneously. The reddening encompasses contributions from both the internal LMC reddening and Galactic foreground reddening, assuming the Seaton reddening law (Seaton 1979) with $E_{b-v} = 0.03$ mag for the latter. The remaining LMC excess is determined by adjusting the free E_{b-v} parameter of the LMC reddening law determined by Howarth (1983).

Since the stellar flux in the optical and IR depends roughly linearly on the stellar temperature (Rayleigh-Jeans domain), the error in T_* (±0.05 dex, see above) influences the luminosity estimate directly. Additional uncertainties are inferred from the reddening correction, which is relatively small for our LMC stars, the imperfect SED fit, and the error margins of the photometry. These errors combine to a final accuracy of about ±0.1 dex in $\log(L/L_\odot)$ for those stars where photometry and flux-calibrated spectra are available. If only photometry is accessible, the accuracy is reduced to ±0.2 dex, due to a larger uncertainty in the SED fit.

5. Results

5.1. Stellar parameters

The analysis of the line spectrum yields the stellar temperature and the "transformed radius" as an immediate result from the PoWR models (cf. Sect. 4). The obtained values are compiled in Table 2 for all stars. Note that the parameters obtained for the binaries and binary candidates in our sample are biased, since we analyzed the spectra as if they were from a single star. A detailed analysis that accounts for the composite nature of these spectra is planned for a forthcoming paper.

The location of the WN stars in the $\log T_*$-$\log R_t$-plane is shown in Fig. 5, omitting the binaries (even the questionable ones). The two parameters ($\log T_*$ and $\log R_t$) appear well correlated, although there is some scatter that exceeds their error margins. Compared to the corresponding diagram for the Galactic WN stars (cf. Fig. 2 in HGL06), the correlation is similar, while the LMC stars cover wider range of spectral subtypes at the cool end (WN10-11).

The WN atmospheres are dominated by helium, while hydrogen is generally depleted. The precise determination of the hydrogen abundance is delicate, because all H lines are blended with He II lines due to the wind broadening. Among the assumably 63 single WN stars of our sample, we find 27 stars where hydrogen is below detectability (see Table 2). The detection limit depends on the individual circumstances such as stellar parameters, quality of the observation, and consistency of the fit. Based on our experience, we estimate that hydrogen abundances higher than 0.05 (mass fraction) do not escape detection.

Line contributions from hydrogen can be found in the spectra of 36 putatively single WN stars, including the four Of/WN stars. There are about equal numbers of stars that fall into the 0.2 and the 0.4 category, respectively.

Overall, Fig. 5 shows a clear dichotomy regarding the hydrogen abundance. Hydrogen is typically undetectable in the hotter stars (early subtypes, WNE), while in the cooler stars (late subtypes, WNL) hydrogen is clearly present, albeit depleted. This pattern is similar to the one found for the Galactic WN stars (HGL06). Even the rough equality between the numbers of WN stars with and without hydrogen is similar to the Galactic sample.

Based on the obtained luminosity, we estimate the current stellar mass using the mass-luminosity relations for chemically homogeneous stars from Gräfener et al. (2011). For stars with hydrogen at their surface, we use their Eq. 9 for core H-burning stars, and for stars without hydrogen we use Eq. 10 for core He-burning stars. Among the putatively single stars, eight stars (BAT99 33, 97, 98, 106, 108, 109, 110, 117) exhibit current stellar masses in excess of 100 $M_\odot$ and thus belong to the category of very massive stars (Vink et al. 2013).

In recent years, evidence is growing that canonical upper mass limit (150 $M_\odot$) is exceeded (e.g., Crowther et al. 2010; Vink et al. 2013). In their study of the stellar population in the core of R136, Crowther et al. (2010) argued in favor of an upper mass limit that is roughly two times the canonical value. Although we achieve slightly lower values in our new analysis, we can confirm the range of stellar masses derived by these authors.

In addition to the stellar parameters listed in Table 2, we have compiled in Table A.3 the number of hydrogen and helium ionizing photons for each star as well as the corresponding Zanstra temperatures. These values have been derived from the ionizing flux of the best fitting model. In some cases however, the stellar wind is so opaque that only an insignificant number of ionizing photons can escape.

5.2. Mass-loss rates

Mass loss of massive stars, especially WR stars, is of key importance for understanding their evolution and their influence on their environment. The huge injection of nuclear-enriched material is one of the main drivers of the chemical evolution of their host clusters and galaxies. For the evolution of WR stars, mass loss can be more important than nuclear fuel consumption.

The mass-loss rates obtained from our analyses are given in Table 2. One must keep in mind that the empirical $\dot{M}$ scales with the square-root of the clumping contrast, $\sqrt{D}$. The value $D = 10$ is not accurately constrained, and may in fact vary from star to star or as function of radius (Nugis et al. 1998; Puls et al. 2006; Liermann & Hamann 2008).

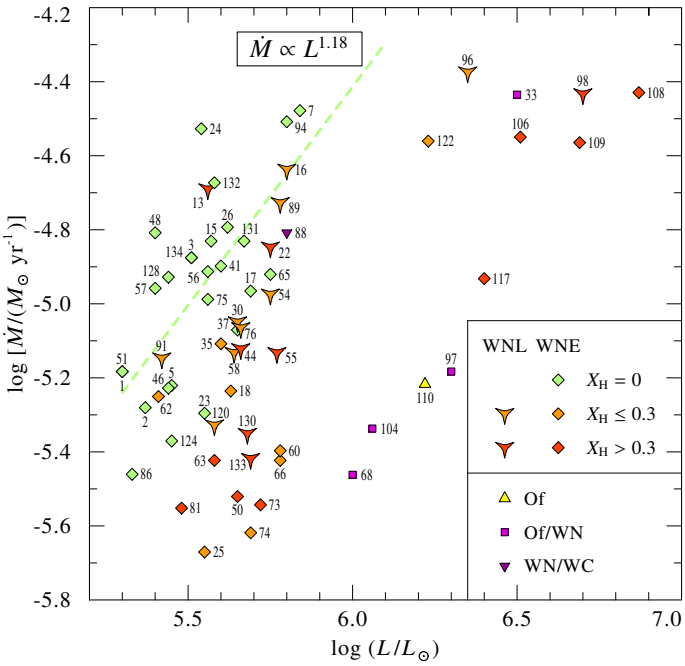

Fig. 6. Mass-loss rates versus luminosity for the putatively single WN stars. The symbol shapes refer to the WNE and WNL subclass, respectively. The atmospheric hydrogen mass fraction is color-coded, as indicated in the inlet. Also shown is a fit (green dashed line) to the hydrogen-free WNE stars.

In Fig. 6, we plot the inferred mass-loss rates versus the luminosities of our sample stars. There is no simple correlation, but there is a characteristic pattern. The very luminous stars ($\log(L/L_\odot) > 6.0$), which all show atmospheric hydrogen, have the highest mass-loss rates ($\log(\dot{M}/(M_\odot/\mathrm{yr})) \approx -4.5$). These stars may be very massive stars directly evolving off the main sequence, possibly still burning hydrogen. However, there are also three Of/WN-type stars with luminosities ≥ 6.0 dex that have weaker winds.

The bulk of "proper" WN stars populate the luminosity range from $\log(L/L_\odot) = 5.3$ to 5.8. Their mass-loss rates scatter over more than one order of magnitude (from -5.7 dex to -4.5 dex), but in clear correlation with the hydrogen abundance. The hydrogen-free stars, which are obviously helium burners, exhibit the strongest winds. Their $\log \dot{M}$ can be fitted to a linear relation with $\log L$, giving

$$\dot{M} = \left(\frac{L}{10^6\ L_\odot}\right)^{1.18} 10^{-4.42}\ M_\odot/\mathrm{yr}\ . \quad (3)$$

In the luminosity range below 5.9 dex, the mass-loss rates of those WN stars, which show a detectable amount of atmospheric hydrogen, scatter a significantly. Nevertheless, it seems that the "proper" WN stars increase their mass-loss rates while evolving toward the Eddington limit, in line with hydrodynamical models calculated by Gräfener & Hamann (2008).

Table 2 also gives the wind efficiency η, defined as the ratio between the rates of the wind momentum, $\dot{M}v_\infty$, and of the momentum of the radiation field, L/c:

$$\eta := \frac{\dot{M}v_\infty c}{L}\ . \quad (4)$$

Wind efficiencies exceeding unity (the "single scattering limit") imply that an average photon undergoes multiple scatterings in the wind. Only specific hydrodynamic wind models can account for this effect. Gräfener & Hamann (2005) obtained $\eta = 2.5$ for a model of the Galactic WC star WR 111. More adequate for our sample, Gräfener & Hamann (2008) calculated WN models for different metallicities and found that, under LMC conditions, the wind efficiency hardly exceeds unity. The empirical wind efficiencies obtained from our analysis are also moderate; the average values (only for the single stars) are 0.8 for the WNL and 2.1 for the WNE subtypes, respectively.

The mass-loss rates of the WN stars in the LMC obtained in the present study can be compared with those of the Galactic WN stars from Hamann et al. (2006). Note that different values for the clumping contrast have been adopted in these studies (LMC: $D = 10$, MW: $D = 4$). Since the empirical $\dot{M}$ depends on the degree of clumping, one must assume for such a comparison that the clumping properties do not differ between the LMC and MW, and scale the mass-loss rates according to Eq. (2).

The comparison reveals that the WN stars in the LMC have on average lower mass-loss rates by roughly a factor of two compared to their Galactic counterparts. This is consistent with a dependence of $\dot{M}$ with metallicity Z to the power 0.9 ± 0.3, depending on the metallicity assumed for the LMC and the MW. This agrees well with the results obtained by Crowther (2006) as well as the exponent 0.86 theoretically derived by Vink & de Koter (2005) for late-type WR stars. A detailed investigation of the mass-loss rate as a function of the metallicity will be the subject of a forthcoming paper, where we will incorporate the results from our study of the WN stars in the SMC.

5.3. The Hertzsprung-Russell diagram

The Hertzsprung-Russell diagram (HRD, Fig. 7) shows all stars analyzed in this paper. Notably, the diagram includes those stars that are already known to be binaries, but were analyzed here as if they were single stars. The highest luminosities in the HRD refer to such multiple stars.

In a second version of the HRD (Fig. 8), we restrict the sample to the WN single stars (including the Of/WN types). While the LMC stars are represented by color-filled symbols, the open symbols in the background are the Galactic WN stars analyzed by HGL06, Martins et al. (2008), Liermann et al. (2010), and Barniske et al. (2008).

One of the striking features in the HRD is the occurrence of a few extremely luminous stars. All these stars show atmospheric hydrogen. In the Galactic sample, there is also a detached group of very luminous stars, but the most luminous WN star encountered in the Galaxy – the "Peony star" WR 102ka (Barniske et al. 2008), reaches only about 6.5 dex solar luminosities.

The very luminous WN stars in the LMC are mostly of early subtypes (WNE) or Of/WN, while the Galactic ones are WNL types. Moreover, the number of WN stars in the high-luminosity domain seems to be much larger in the Galactic sample. This might actually indicate a problem with the Galactic analyses that arises from the uncertainty of the stellar distances. Many of these Galactic WNL stars were "brightness calibrated" by means of those few WNL representatives that belong to clusters or associations. However, these young WNL stars may be exceptionally luminous. By employing them for the brightness calibration, the luminosities of other Galactic WNL stars might have been overestimated. Due to the known distance, the LMC results are free from such uncertainties.

Based on their known, uniform distance, we can now check for our LMC stars if such relation between absolute brightness and spectral subtype really exists. As Fig. 9 reveals, there is indeed some correlation, but the scatter within each subtype is

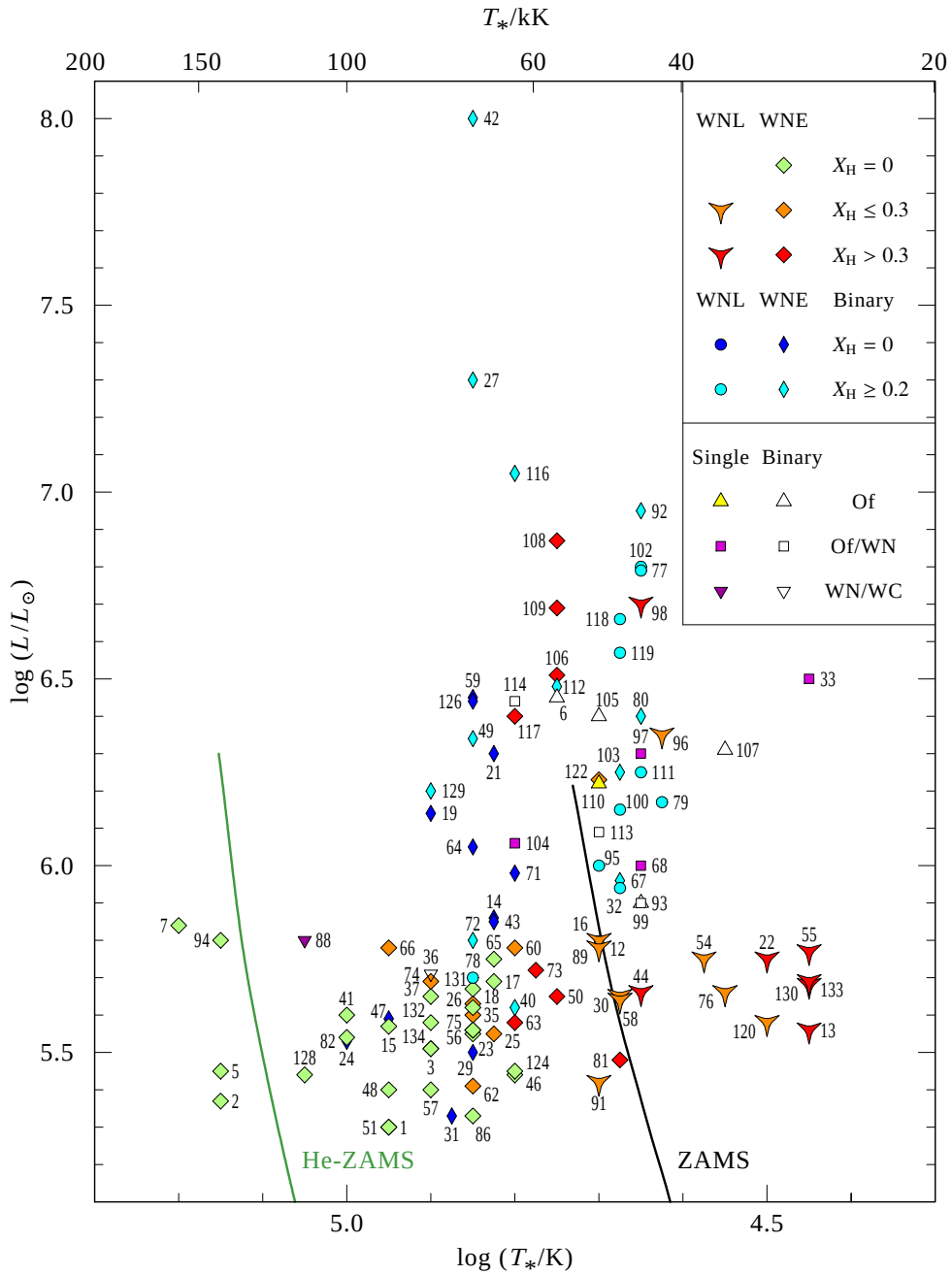

Fig. 7. The HRD of our sample of LMC stars. As explained in the inlet, different symbols represent WNL and WNE stars, respectively. Binaries are also included, but distinguished by different symbols; their spectra have been analyzed as if they were single stars. The five O-type stars in our sample are plotted with their own symbols. Among the WN stars, the color codes the hydrogen mass fraction as defined in the inlet. The zero-age main sequences (ZAMS) for hydrogen-rich and pure-helium stars are shown for orientation.

large (1 mag, typically). The relation obtained by linear regression (thick shaded lines in Fig. 9) for the WNE stars is similar to the one adopted in Hamann et al. (2006), while the hydrogen-containing WNL stars in the LMC are on average less bright than $M_v = -7.22$ mag as used for the Galactic calibration. We note that the highest M_v is associated with BAT99 98, which we treat as a single star, although the moderate fit quality might indicate a hidden companion (cf. Appendix B). The average M_v value of each WN subtype is compiled in Table 3.

The bulk of "proper" WN stars populate the luminosity range from $\log(L/L_\odot) = 5.3$ to 5.8. The hydrogen containing stars are mainly found on the cool side of the zero-age main-sequence (ZAMS), where all WN stars are of late subtypes (WNL). The hydrogen-free stars, all of early subtypes (WNE), gather at the hot side of the ZAMS and near the theoretical zero-age main-sequence for helium stars (He-ZAMS).

In the Galactic sample, the group of WNL stars with hydrogen was not encountered in this luminosity range, possibly because of the erroneous brightness calibration applied to those stars as discussed above.

6. Discussion

Our large sample offers an excellent possibility to compare the almost complete WN population of the LMC with the predictions of the stellar evolution theory. Figure 10 shows the HRD of

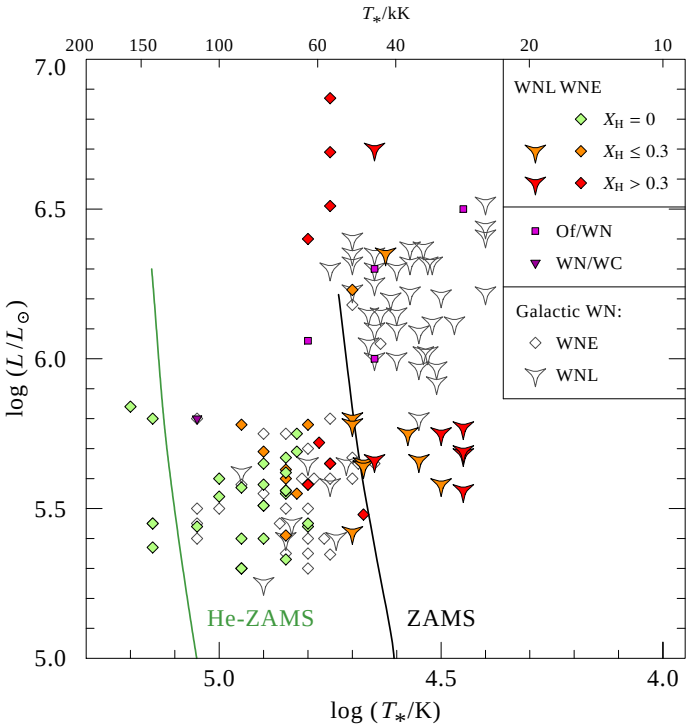

Fig. 8. The HRD of the single WN stars. The color-filled symbols refer to the LMC stars analyzed in the present paper. The open symbols in the background represent the Galactic WN stars for comparison (cf. inlet).

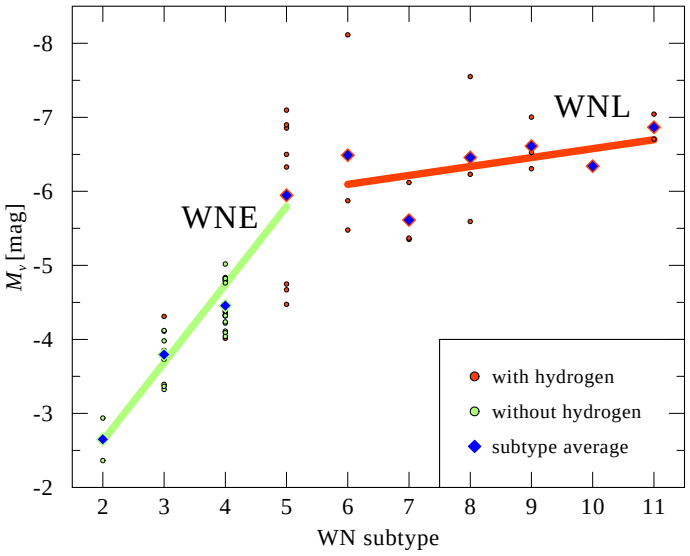

Fig. 9. Absolute visual magnitudes (narrowband color as defined by Smith 1968) versus spectral subtype number for the putatively single stars in our sample. Colors code the absence (green/light) or presence (red/dark) of hydrogen. While small symbols represent individual stars, the thick symbols mark the average M_v of each subtype. The thick lines indicate linear fits to the early (WN2–5) and late (WN6–11) subtypes, respectively.

our program stars in comparison to the stellar evolution tracks calculated by the Geneva group for LMC metallicity. In the version shown here, stellar evolution models account for the effects of rotation, but neglect the metallicity scaling in the WR phase (Meynet & Maeder 2005).

The individual evolution phases are distinguished by different drawing styles, according to the chemical composition at the stellar surface. At hydrogen surface abundances $X_H > 0.4$ (mass fraction), the star is considered to be in a pre-WR phase represented by a thin black line. The WNL stage, which per definition initiates when the hydrogen abundance drops below 0.4 (mass fraction) in the atmosphere, is highlighted by thick red lines. Hydrogen abundances below 0.05 (mass fraction) are considered to correspond to the WNE stage, and the track is plotted as a thick green line. Finally, for carbon abundances above 0.2 (mass fraction), the star reaches the WC and WO phase and the track is drawn as a gray line.

Table 3. Averaged absolute visual magnitudes of each WN subtype

Subtype	M_v	σ_{M_v}
WN 2	−2.65	0.29
WN 3	−3.8	0.31
WN 4	−4.46	0.3
WN 5	−5.95	1.05
WN 6	−6.49	1.16
WN 7	−5.61	0.36
WN 8	−6.46	0.82
WN 9	−6.61	0.29
WN 10	−6.34	-
WN 11	−6.87	0.14

Until now, we classified stars as WNE and WNL according to their spectroscopic subtype. With regard to stellar evolution, the terms "WNE" and "WNL" are defined differently and refer only to the atmospheric composition, i.e., the absence or presence of hydrogen. Note also that the temperature axis in Fig. 10 refers to the stellar temperature, i.e., to the effective temperature related to the hydrostatic core, but not to the photosphere (cf. Sect. 3).

Let us first look at the very luminous stars, separated from the others by a gap at about $\log(L/L_\odot) = 5.9$. These stars can be explained by tracks similar to the one for 120 $M_\odot$ shown in Fig. 10. This track stays close to the ZAMS, increases in luminosity until it enters the WNL stage, then drops, and finally evolves toward the helium main sequence after having lost all hydrogen. While the highest initial mass for which tracks are provided by Meynet & Maeder (2005) is 120 $M_\odot$, the most luminous star of this group (BAT99 108), if indeed a single star, requires about 300 $M_\odot$, as already pointed out by Crowther et al. (2010).

Similar to the WN stars in the Galaxy, only objects with a substantial amount of hydrogen are found at luminosities of $\log(L/L_\odot) > 5.9$, although, according to stellar evolution models (Meynet & Maeder 2005; Yusof et al. 2013), hydrogen-free stars are also expected in this parameter regime. This mismatch might be partly explained by very luminous type IIn supernovae (SN). Smith (2008) unveiled that the progenitors of these rare SN are probably high-mass stars ($M_{\rm init} > 50\ M_\odot$) that explode with a significant amount of hydrogen left in their stellar atmospheres. The observational evidence discussed by this author argues for episodic mass loss prior to the type IIn SNe in excess of typical WR mass-loss rates, suggesting that progenitor candidates are classical LBVs. Since the WN stars observed in this mass range seem to be rather normal WN stars, apart from their high luminosities, the origin and fate of the very massive stars still remains puzzling.

With the exception of the 120 $M_\odot$ track, all stellar evolution tracks (for LMC metallicities) presented by Meynet & Maeder (2005) evolve toward the red supergiant (RSG) stage, but barely reach the corresponding temperature range before evolving back

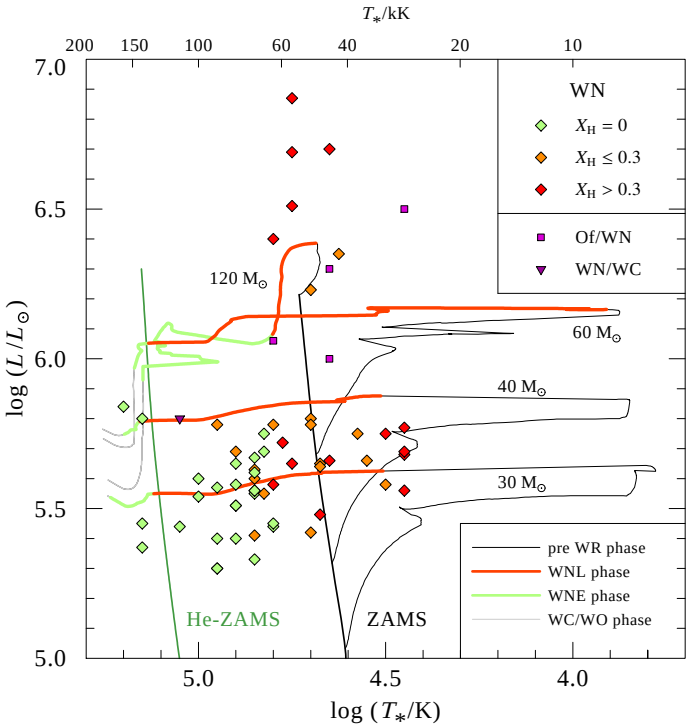

Fig. 10. The HRD with the single WN stars (discrete symbols) and stellar evolution tracks from Meynet & Maeder (2005), which account for the effects of rotation. The labels indicate the initial mass. The color coding of the tracks during the WR phases (thick lines) corresponds to the filling color of the symbols, which reflects the observed atmospheric composition (see inlet).

to the hot part of the HRD. Nevertheless, in this paper, we denote all evolution stages in the cool part of the HRD as RSG even if the tracks only pass the blue supergiant and LBV domain of the HRD. As can be seen in Fig. 10, luminosities of about 6.2 dex are reached by the post RSG evolution of stars with initially 60 $M_\odot$ (Meynet & Maeder 2005). However, no "cool" WNL stars are found in this range, which might indicate that the RSG stage is in fact not reached in this mass range, possibly because of the LBV instability barrier.

The bulk of WN stars are found in the luminosity range $\log(L/L_\odot) = 5.3 \ldots 5.8$. The upper end of this range corresponds quite well to the post-RSG track with initially 40 $M_\odot$. Interestingly, this upper mass limit agrees well with analyses of WC stars in the LMC by Gräfener et al. (1998) and Crowther et al. (2002).

The lowest initial mass for which a post-RSG track is provided by Meynet & Maeder (2005) for LMC metallicities is 30 $M_\odot$. The luminosities of the analyzed WN stars show a lower cutoff at about $10^{5.3}$ $L_\odot$, which rather corresponds to an initial mass of about 20 $M_\odot$. Meynet & Maeder (2005), based on interpolation of their tracks, estimated that the minimum initial mass for reaching WR phases is about 25 $M_\odot$ for LMC metallicity. This limit seems to be too high, compared to our results. The older Geneva tracks, which did not account for rotation (Schaerer et al. 1993), are even more contradictory; these tracks fail to reach post-RSG stages for initial masses below 60$M_\odot$. We also compared our empirical HRD positions with non rotating models from Eldridge & Vink (2006). These models predict WR stars for initial masses exceeding 33$M_\odot$.

As stated in Sect. 1, it is theoretically expected that the evolution of massive stars depends on their initial metallicity. Stellar evolution models predict a higher minimum for the initial mass of WR stars with decreasing metallicity due to the reduced mass loss by stellar winds anticipated at lower metallicities. Indeed, our study shows that the mass-loss rate of an average WN star in the LMC is lower than in the Galaxy (see Sect. 5.2 for details). However, Fig. 8 illustrates that the initial masses for the LMC WN stars are comparable to their Galactic counterparts. Thus, the conventional expectation that WN stars in the LMC originate from a higher mass range compared to their Galactic twins is not supported from our sample.

In the mass range from 20 $M_\odot$ to 40 $M_\odot$, the stellar evolution in the Galaxy and the LMC results in comparable HRD positions for the WN stars, although the mass-loss rates and the metallicity are lower in the LMC. This may be attributed to the relatively small differences between the metallicity of these two galaxies. Another implication might be that the WN stars and their progenitors rotate faster in the LMC than in the Galaxy, because their lower mass-loss rates imply a reduced loss of angular momentum. A faster rotation increases the WR lifetime and decreases the minimum initial mass for the WR phase, mainly due to a more efficient internal mixing (Maeder & Meynet 2005).

Do the stellar evolution calculations successfully predict the observed number ratio between WNE and WNL stars? We used the four tracks from Meynet & Maeder (2005) for computing synthetic populations, assuming a Salpeter initial mass function and a constant star formation rate (see HGL06, for similar simulations of the Galactic WR stars). From our simulations, we expect roughly 20 % of all WN stars in the WNE phase, i.e., much less than the 40 % observed. Even worse, almost half of these WNE stars originate from the tracks for 60 and 120 $M_\odot$ initial mass and thus lie at luminosities where no WNE stars at all are found in our sample.

The synthetic population yields about the same number of WC stars as WNE stars. In fact, the WNE stars residing in the LMC are twice as frequent as the LMC-WC stars. Moreover, half of these WC stars are predicted to evolve from 120 $M_\odot$ initial mass, which does not match the low WC luminosities actually observed (Gräfener et al. 1998; Crowther et al. 2002). Based on stellar evolution models, Eldridge & Vink (2006) show that a better agreement with the observed WC/WN ration can be achieved by means of a metallicity scaling of the mass-loss rate during the WR phase. However, like the Geneva models, these models also fail to reproduce the observed luminosity ranges for the different WR subtypes.

The color-coded evolution tracks in Fig. 10 reveal a discrepancy in stellar temperature between these tracks and the HRD position of the WNE stars. Theoretically, it is expected that the hydrogen-free WNE stars are located on the He-ZAMS. Instead, a clear gap is seen between most of these stars and the He-ZAMS. This discrepancy in the effective temperature is attributed to the long known "radius problem" of hydrogen-free WR stars. The observed WR radii are up to an order of magnitude larger than the radii predicted by stellar evolution models. We note that the effective temperature of the stellar evolution models refer to the hydrostatic core radius whereas the effective temperature of our atmosphere models is defined at the inner boundary radius R_*, where the Rosseland optical depth reaches 20 (cf. Sect. 3). However, this cannot be the decisive reason because R_* is close to the hydrostatic core radius as long as R_* is located in the hydrostatic part of the wind, which is the case for most of our final-fit models. A solution for this radius problem has been studied by Gräfener et al. (2012). These authors show that an inflated subphotospheric layer, which incorporates the ef-

fect of clumping, can bring the observed WR radii in agreement with the theory.

The binaries in our sample have been thoroughly identified, but some may have escaped detection, as discussed in Sect. 2.2. Moreover, a single star could be the product of binary evolution, e.g., a merger or a binary system where the companion already exploded (Sana et al. 2012). The consequences of binary evolution with respect to the population of WR stars have been discussed by various authors (e.g., Paczyński 1967; Vanbeveren et al. 2007; Eldridge et al. 2008, 2013). According to these authors, the minimum initial mass for the WR phases is considerably decreased in binary systems due to a significant pre-WR mass-loss through Roche lobe overflow. If the least luminous stars of our sample had evolved through the binary channel, this would explain the discrepancy with the minimum initial mass of WR stars as predicted from single star evolution.

Alternatively, single star evolution may produce WR stars from lower initial masses when higher initial rotation velocities (more than the 300 km s^{-1} as assumed by Meynet & Maeder 2005) are adopted. More plausibly, mass-loss rates that are enhanced over those usually adopted during the RSG stage promote the evolution of massive stars toward the blue part of the HRD (e.g., Vanbeveren et al. 1998, 2007; Georgy 2012).

Binary evolution was shown to significantly affect the WC/WN ratio (e.g., Vanbeveren et al. 2007; Eldridge et al. 2008). Eldridge et al. (2008) demonstrate that, while their single star models reproduce the observed WC/WN ratio, the binary population models predict too many WN stars. The bias from close binary evolution on the WN population should be subject to future investigations.

The WNE and WC stars are thought to be the progenitors of type Ib and type Ic supernovae (e.g., Gaskell et al. 1986; Begelman & Sarazin 1986), if they do not directly collapse to a black hole without a bright SN. The first tentative identification of a WR star as a type Ib SN progenitor has been reported recently for SN iPTF13bvn (Cao et al. 2013). Alternatively, Eldridge et al. (2013) show that the bulk of the SNe of type Ibc can originate from relatively low-mass pure helium stars whose hydrogen-rich atmospheres have been stripped by close binary interactions. Our empirical HDR positions (Fig. 10) suggest that the LMC-WNE stars and their successors are restricted to initial masses below 40 $M_\odot$ similar to the situation in our Galaxy (cf. Sander et al. 2012).

Summarizing the discussion on stellar evolution, we found some general agreement between our WN analyses and the Geneva tracks for LMC metallicity that account for stellar rotation (Meynet & Maeder 2005). However, in a quantitative sense, the stellar evolution tracks are not consistent with our empirical results. The discrepancies refer especially to the range of initial masses required for reaching the respective WR phases, and to the number ratios and luminosities of the different WR subtypes. Interestingly, similar conclusions have been drawn from our study of the Galactic WN stars and the comparison with the corresponding Geneva tracks (HGL06). Moreover, Sander et al. (2012) analyzed the Galactic WC stars and found that their relatively low luminosities are not reproduced by the Geneva tracks. Calculations by Vanbeveren et al. (1998), who adopted higher mass-loss rates during the RSG stage, yielded a better agreement. We may also mention here the work of Hunter et al. (2008), who determined the chemical composition of 135 early B-type stars in the LMC to test the prediction of rotationally induced mixing. They demonstrated that about 40 % of their sample do not agree with the predicted correlation between rotation and nitrogen enrichment. Hence it seems that massive-star evolution is still not fully understood.

7. Summary and Conclusions

1. The spectra of 107 stars in the LMC have been analyzed by means of state-of-the-art model atmospheres.
2. The sample contains 102 WR stars of the nitrogen sequence (WN, including five Of/WN), and thus comprises nearly the complete population of WN stars known in the LMC.
3. Of these WN stars, 63 do not show any indications of multiplicity, and thus are putatively single stars.
4. Two groups of WN stars can be distinguished from their luminosity: a small group (12 %) of very luminous stars $\log(L/L_\odot) > 5.9$, and a large group (88 %) populating the range of moderate luminosities between $\log(L/L_\odot) = 5.3 ... 5.8$.
5. Of the 63 single, 27 WN stars (i.e., 43 %) do not show hydrogen in their wind. These hydrogen-free stars are only found in the group with moderate luminosities.
6. Stellar radii are generally larger, and effective temperatures correspondingly lower, than predicted from stellar evolution models. This may indicate a subphotospheric inflation, as discussed in the recent literature.
7. The bulk of WN stars (with moderate luminosities) seem to be in a post-RSG evolution phase.
8. According to their luminosities in the range $\log(L/L_\odot) = 5.3 ... 5.8$, these WN stars originate from initial stellar masses between 20 $M_\odot$ and 40 $M_\odot$. This mass range is similar to the range found for the Galaxy. Hence, the expected metallicity dependence of the evolution is not seen.
9. Stellar evolution tracks, when accounting for rotationally induced mixing, in principle, can explain the extremely luminous WN stars as well as the bulk of WN stars with moderate luminosities. The former evolve directly from the ZAMS, while the latter go through the RSG stage. However, the stellar evolution models still fail to correctly reproduce the observed ranges of luminosities and initial masses.

Acknowledgements. We would like to thank the referee, John Eldridge, for his constructive comments that have significantly improved the present work. This research made use of the SIMBAD database, operated at CDS, Strasbourg, France, and of data products from the Two Micron All Sky Survey, which is a joint project of the University of Massachusetts and the Infrared Processing and Analysis Center/California Institute of Technology, funded by the National Aeronautics and Space Administration and the National Science Foundation (NASA). This work is partly based on INES data from the IUE satellite, and on observations with the Spitzer Space Telescope, which is operated by the Jet Propulsion Laboratory, California Institute of Technology under a contract with NASA. This research made also use of NASA's Astrophysics Data System and of the VizieR catalog access tool, CDS, Strasbourg, France. Some of the data presented in this paper were retrieved from the Mikulski Archive for Space Telescopes (MAST). STScI is operated by the Association of Universities for Research in Astronomy, Inc., under NASA contract NAS5-26555. Support for MAST for non-HST data is provided by the NASA Office of Space Science via grant NNX09AF08G. The work also based on data made available through Wikimbad, hosted in the LAOG, France (http://wikimbad.org). LMO acknowledges the funding by DLR grant 50 OR 1302.

References

Allen, D. A. & Glass, I. S. 1976, ApJ, 210, 666
Asplund, M., Grevesse, N., Sauval, A. J., & Scott, P. 2009, ARA&A, 47, 481
Barlow, M. J. & Hummer, D. G. 1982, in IAU Symposium, Vol. 99, Wolf-Rayet Stars: Observations, Physics, Evolution, ed. C. W. H. De Loore & A. J. Willis, 387–392
Barniske, A., Oskinova, L. M., & Hamann, W.-R. 2008, A&A, 486, 971
Begelman, M. C. & Sarazin, C. L. 1986, ApJ, 302, L59

Bonanos, A. Z., Massa, D. L., Sewilo, M., et al. 2009, AJ, 138, 1003
Breysacher, J. 1981, A&AS, 43, 203
Breysacher, J. 1986, A&A, 160, 185
Breysacher, J., Azzopardi, M., & Testor, G. 1999, A&AS, 137, 117
Cao, Y., Kasliwal, M. M., Arcavi, I., et al. 2013, ApJ, 775, L7
Chené, A.-N., Moffat, A. F. J., Cameron, C., et al. 2011, ApJ, 735, 34
Chini, R., Hoffmeister, V. H., Nasseri, A., Stahl, O., & Zinnecker, H. 2012, MNRAS, 424, 1925
Cowley, A. P., Crampton, D., Hutchings, J. B., & Thompson, I. B. 1984, PASP, 96, 968
Cowley, A. P. & Hutchings, J. B. 1978, PASP, 90, 636
Crowther, P. A. 2006, in Astronomical Society of the Pacific Conference Series, Vol. 353, Stellar Evolution at Low Metallicity: Mass Loss, Explosions, Cosmology, ed. H. J. G. L. M. Lamers, N. Langer, T. Nugis, & K. Annuk, 157
Crowther, P. A. & Dessart, L. 1998, MNRAS, 296, 622
Crowther, P. A., Dessart, L., Hillier, D. J., Abbott, J. B., & Fullerton, A. W. 2002, A&A, 392, 653
Crowther, P. A. & Hadfield, L. J. 2006, A&A, 449, 711
Crowther, P. A., Hillier, D. J., & Smith, L. J. 1995a, A&A, 293, 172
Crowther, P. A., Schnurr, O., Hirschi, R., et al. 2010, MNRAS, 408, 731
Crowther, P. A. & Smith, L. J. 1997, A&A, 320, 500
Crowther, P. A., Smith, L. J., & Willis, A. J. 1995b, A&A, 304, 269
Crowther, P. A. & Walborn, N. R. 2011, MNRAS, 416, 1311
Cutri, R. M., Skrutskie, M. F., van Dyk, S., et al. 2012, VizieR Online Data Catalog, 2281, 0
Dalton, G. B., Caldwell, M., Ward, A. K., et al. 2006, in Society of Photo-Optical Instrumentation Engineers (SPIE) Conference Series, Vol. 6269, Society of Photo-Optical Instrumentation Engineers (SPIE) Conference Series
de Koter, A., Heap, S. R., & Hubeny, I. 1997, ApJ, 477, 792
Dopita, M. A., Bell, J. F., Chu, Y.-H., & Lozinskaya, T. A. 1994, ApJS, 93, 455
Doran, E. I. & Crowther, P. A. 2011, Bulletin de la Societe Royale des Sciences de Liege, 80, 129
Doran, E. I., Crowther, P. A., de Koter, A., et al. 2013, A&A, 558, A134
Duflot, M. 2010, VizieR Online Data Catalog, 5131, 0
Dufour, R. J., Shields, G. A., & Talbot, Jr., R. J. 1982, ApJ, 252, 461
Eldridge, J. J., Fraser, M., Smartt, S. J., Maund, J. R., & Crockett, R. M. 2013, MNRAS, 436, 774
Eldridge, J. J., Izzard, R. G., & Tout, C. A. 2008, MNRAS, 384, 1109
Eldridge, J. J. & Vink, J. S. 2006, A&A, 452, 295
Emerson, J., McPherson, A., & Sutherland, W. 2006, The Messenger, 126, 41
Evans, C. J., Taylor, W. D., Hénault-Brunet, V., et al. 2011, A&A, 530, A108
Foellmi, C., Moffat, A. F. J., & Guerrero, M. A. 2003a, MNRAS, 338, 360
Foellmi, C., Moffat, A. F. J., & Guerrero, M. A. 2003b, MNRAS, 338, 1025
Foellmi, C., Moffat, A. F. J., & Marchenko, S. V. 2006, A&A, 447, 667
Gamen, R., Gosset, E., Morrell, N., et al. 2006, A&A, 460, 777
Gaskell, C. M., Cappellaro, E., Dinerstein, H. L., et al. 1986, ApJ, 306, L77
Georgy, C. 2012, A&A, 538, L8
Girard, T. M., van Altena, W. F., Zacharias, N., et al. 2011, AJ, 142, 15
Glass, I. S. 1984, MNRAS, 209, 759
Gosset, E., Nazé, Y., Claeskens, J.-F., et al. 2005, A&A, 429, 685
Gräfener, G. & Hamann, W.-R. 2005, A&A, 432, 633
Gräfener, G. & Hamann, W.-R. 2007, in Astronomical Society of the Pacific Conference Series, Vol. 367, Massive Stars in Interactive Binaries, ed. N. St.-Louis & A. F. J. Moffat, 131
Gräfener, G. & Hamann, W.-R. 2008, A&A, 482, 945
Gräfener, G., Hamann, W.-R., Hillier, D. J., & Koesterke, L. 1998, A&A, 329, 190
Gräfener, G., Koesterke, L., & Hamann, W.-R. 2002, A&A, 387, 244
Gräfener, G., Owocki, S. P., & Vink, J. S. 2012, A&A, 538, A40
Gräfener, G., Vink, J. S., de Koter, A., & Langer, N. 2011, A&A, 535, A56
Guerrero, M. A. & Chu, Y.-H. 2008a, ApJS, 177, 216
Guerrero, M. A. & Chu, Y.-H. 2008b, ApJS, 177, 238
Gvaramadze, V. V., Kniazev, A. Y., & Fabrika, S. 2010, MNRAS, 405, 1047
Hamann, W.-R. & Gräfener, G. 2004, A&A, 427, 697
Hamann, W.-R., Gräfener, G., & Liermann, A. 2006, A&A, 457, 1015
Hamann, W.-R. & Koesterke, L. 1998, A&A, 335, 1003
Hamann, W.-R. & Koesterke, L. 2000, A&A, 360, 647
Haschke, R., Grebel, E. K., & Duffau, S. 2011, AJ, 141, 158
Heap, S. R., Altner, B., Ebbets, D., et al. 1991, ApJ, 377, L29
Heap, S. R., Ebbets, D., Malumuth, E. M., et al. 1994, ApJ, 435, L39
Heger, A. & Langer, N. 2000, ApJ, 544, 1016
Heydari-Malayeri, M., Courbin, F., Rauw, G., Esslinger, O., & Magain, P. 1997, A&A, 326, 143
Hillier, D. J. 1991, A&A, 247, 455
Hillier, D. J. & Miller, D. L. 1999, ApJ, 519, 354
Howarth, I. D. 1983, MNRAS, 203, 301
Humphreys, R. M. & Davidson, K. 1994, PASP, 106, 1025
Hunter, I., Brott, I., Lennon, D. J., et al. 2008, ApJ, 676, L29
Hunter, I., Dufton, P. L., Smartt, S. J., et al. 2007, A&A, 466, 277
Hyland, A. R., Thomas, J. A., & Robinson, G. 1978, AJ, 83, 20
Ignace, R., Oskinova, L. M., & Brown, J. C. 2003, A&A, 408, 353
Ignace, R., Oskinova, L. M., & Foullon, C. 2000, MNRAS, 318, 214
Kato, D., Nagashima, C., Nagayama, T., et al. 2007, PASJ, 59, 615
Koenigsberger, G., Moffat, A. F. J., & Auer, L. H. 2003, Rev. Mexicana Astron. Astrofis., 39, 213
Koesterke, L., Hamann, W.-R., Wessolowski, U., & Schmutz, W. 1991, A&A, 248, 166
Korn, A. J., Nieva, M. F., Daflon, S., & Cunha, K. 2005, ApJ, 633, 899
Kudritzki, R. P., Pauldrach, A., Puls, J., & Abbott, D. C. 1989, A&A, 219, 205
Kurt, C. M. & Dufour, R. J. 1998, in Revista Mexicana de Astronomia y Astrofisica Conference Series, Vol. 7, Revista Mexicana de Astronomia y Astrofisica Conference Series, ed. R. J. Dufour & S. Torres-Peimbert, 202
Larsen, S. S., Clausen, J. V., & Storm, J. 2000, A&A, 364, 455
Liermann, A. & Hamann, W.-R. 2008, in Clumping in Hot-Star Winds, ed. W.-R. Hamann, A. Feldmeier, & L. M. Oskinova, 247
Liermann, A., Hamann, W.-R., Oskinova, L. M., Todt, H., & Butler, K. 2010, A&A, 524, A82
Lommen, D., Yungelson, L., van den Heuvel, E., Nelemans, G., & Portegies Zwart, S. 2005, A&A, 443, 231
Madore, B. F. & Freedman, W. L. 1998, ApJ, 492, 110
Maeder, A. & Meynet, G. 2005, A&A, 440, 1041
Martín-Hernández, N. L., Vermeij, R., & van der Hulst, J. M. 2005, A&A, 433, 205
Martins, F., Hillier, D. J., Paumard, T., et al. 2008, A&A, 478, 219
Massey, P. 2002, ApJS, 141, 81
Massey, P., Puls, J., Pauldrach, A. W. A., et al. 2005, ApJ, 627, 477
Massey, P., Waterhouse, E., & DeGioia-Eastwood, K. 2000, AJ, 119, 2214
Meynet, G. & Maeder, A. 2003, A&A, 404, 975
Meynet, G. & Maeder, A. 2005, A&A, 429, 581
Moffat, A. F. J. 1989, ApJ, 347, 373
Moffat, A. F. J., Niemela, V. S., Phillips, M. M., Chu, Y.-H., & Seggewiss, W. 1987, ApJ, 312, 612
Nazé, Y., Rauw, G., Manfroid, J., Chu, Y.-H., & Vreux, J.-M. 2003a, A&A, 401, L13
Nazé, Y., Rauw, G., Manfroid, J., Chu, Y.-H., & Vreux, J.-M. 2003b, A&A, 408, 171
Neugent, K. F., Massey, P., & Morrell, N. 2012, AJ, 144, 162
Niedzielski, A., Nugis, T., & Skorzynski, W. 2004, Acta Astronomica, 54, 405
Niedzielski, A. & Skorzynski, W. 2002, Acta Astronomica, 52, 81
Niemela, V. S. 1991, in IAU Symposium, Vol. 143, Wolf-Rayet Stars and Interrelations with Other Massive Stars in Galaxies, ed. K. A. van der Hucht & B. Hidayat, 201
Niemela, V. S., Seggewiss, W., & Moffat, A. F. J. 1995, in IAU Symposium, Vol. 163, Wolf-Rayet Stars: Binaries; Colliding Winds; Evolution, ed. K. A. van der Hucht & P. M. Williams, 251
Niemela, V. S., Seggewiss, W., & Moffat, A. F. J. 2001, A&A, 369, 544
Nota, A., Pasquali, A., Drissen, L., et al. 1996, ApJS, 102, 383
Nugis, T., Crowther, P. A., & Willis, A. J. 1998, A&A, 333, 956
O'Connell, R. 2008, in HST Proposal, 11360
Oskinova, L. M., Gayley, K. G., Hamann, W.-R., et al. 2012, ApJ, 747, L25
Oskinova, L. M., Ignace, R., Hamann, W.-R., Pollock, A. M. T., & Brown, J. C. 2003, A&A, 402, 755
Paczyński, B. 1967, Acta Astron., 17, 355
Parker, J. W. 1993, AJ, 106, 560
Pasquali, A., Langer, N., Schmutz, W., et al. 1997, ApJ, 478, 340
Pasquali, A., Nota, A., & Clampin, M. 1999, A&A, 343, 536
Pauldrach, A., Puls, J., & Kudritzki, R. P. 1986, A&A, 164, 86
Pauldrach, A. W. A., Kudritzki, R. P., Puls, J., Butler, K., & Hunsinger, J. 1994, A&A, 283, 525
Piatti, A. E. & Geisler, D. 2013, AJ, 145, 17
Pietrzyński, G., Graczyk, D., Gieren, W., et al. 2013, Nature, 495, 76
Puls, J., Markova, N., Scuderi, S., et al. 2006, A&A, 454, 625
Puls, J., Urbaneja, M. A., Venero, R., et al. 2005, A&A, 435, 669
Raassen, A. J. J., van der Hucht, K. A., Mewe, R., et al. 2003, A&A, 402, 653
Reid, W. A. & Parker, Q. A. 2012, MNRAS, 425, 355
Sana, H., de Koter, A., de Mink, S. E., et al. 2013a, A&A, 550, A107
Sana, H., de Mink, S. E., de Koter, A., et al. 2012, Science, 337, 444
Sana, H., van Boeckel, T., Tramper, F., et al. 2013b, MNRAS, 432, L26
Sander, A., Hamann, W.-R., & Todt, H. 2012, A&A, 540, A144
Schaerer, D., Meynet, G., Maeder, A., & Schaller, G. 1993, A&AS, 98, 523
Schmutz, W., Hamann, W., & Wessolowski, U. 1989, A&A, 210, 236
Schmutz, W., Leitherer, C., Hubeny, I., et al. 1991, ApJ, 372, 664
Schnurr, O., Chené, A.-N., Casoli, J., Moffat, A. F. J., & St-Louis, N. 2009a, MNRAS, 397, 2049
Schnurr, O., Moffat, A. F. J., St-Louis, N., Morrell, N. I., & Guerrero, M. A. 2008, MNRAS, 389, 806
Schnurr, O., Moffat, A. F. J., Villar-Sbaffi, A., St-Louis, N., & Morrell, N. I. 2009b, MNRAS, 395, 823
Seaton, M. J. 1979, MNRAS, 187, 73P
Seggewiss, W., Moffat, A. F. J., & Lamontagne, R. 1991, A&AS, 89, 105

Selman, F., Melnick, J., Bosch, G., & Terlevich, R. 1999, A&A, 341, 98
Shenar, T., Hamann, W.-R., & Todt, H. 2014, A&A, 562, A118
Skinner, S. L., Zhekov, S. A., Güdel, M., Schmutz, W., & Sokal, K. R. 2012, AJ, 143, 116
Skrutskie, M. F., Cutri, R. M., Stiening, R., et al. 2006, AJ, 131, 1163
Smith, L. F. 1968, MNRAS, 140, 409
Smith, L. F., Shara, M. M., & Moffat, A. F. J. 1996, MNRAS, 281, 163
Smith, L. J., Norris, R. P. F., & Crowther, P. A. 2002, MNRAS, 337, 1309
Smith, N. 2008, in IAU Symposium, Vol. 250, IAU Symposium, ed. F. Bresolin, P. A. Crowther, & J. Puls, 193–200
Smith, R. C., Points, S., Chu, Y.-H., et al. 2005, in Bulletin of the American Astronomical Society, Vol. 37, American Astronomical Society Meeting Abstracts, #145.01
Stahl, O., Wolf, B., Leitherer, C., et al. 1984, A&A, 140, 459
Stevens, I. R., Blondin, J. M., & Pollock, A. M. T. 1992, ApJ, 386, 265
Subramaniam, A. 2005, A&A, 430, 421
Taylor, W. D., Evans, C. J., Sana, H., et al. 2011, A&A, 530, L10
Testor, G., Llebaria, A., & Debray, B. 1988, The Messenger, 54, 43
Todt, H., Kniazev, A. Y., Gvaramadze, V. V., et al. 2013, MNRAS, 430, 2302
Torres-Dodgen, A. V. & Massey, P. 1988, AJ, 96, 1076
Townsley, L. K., Broos, P. S., Feigelson, E. D., Garmire, G. P., & Getman, K. V. 2006, AJ, 131, 2164
Trundle, C., Dufton, P. L., Hunter, I., et al. 2007, A&A, 471, 625
Vanbeveren, D., De Donder, E., van Bever, J., van Rensbergen, W., & De Loore, C. 1998, New A, 3, 443
Vanbeveren, D., Van Bever, J., & Belkus, H. 2007, ApJ, 662, L107
Vink, J. S. 2007, A&A, 469, 707
Vink, J. S. & de Koter, A. 2005, A&A, 442, 587
Vink, J. S., Heger, A., Krumholz, M. R., et al. 2013, ArXiv e-prints
Walborn, N. R. 1982, ApJ, 256, 452
Walborn, N. R., Drissen, L., Parker, J. W., et al. 1999, AJ, 118, 1684
Walborn, N. R., MacKenty, J. W., Saha, A., White, R. L., & Parker, J. W. 1995, ApJ, 439, L47
Weis, K. 2003, A&A, 408, 205
Willis, A. J., Crowther, P. A., Fullerton, A. W., et al. 2004, ApJS, 154, 651
Yoon, S.-C., Dierks, A., & Langer, N. 2012, A&A, 542, A113
Yusof, N., Hirschi, R., Meynet, G., et al. 2013, MNRAS, 433, 1114
Zaritsky, D., Harris, J., Thompson, I. B., & Grebel, E. K. 2004, AJ, 128, 1606

Table 2. Parameters of LMC WN stars

BAT99	Subtype	Ref.	T_* [kK]	$\log R_t$ [$R_\odot$]	v_∞ [km/s]	E_{b-v} [mag]	M_v [mag]	R_* [$R_\odot$]	$\log \dot{M}$ [$M_\odot$/yr]	$\log L$ [$L_\odot$]	η	M^a [$M_\odot$]	X_H	Bin.[b]	Ref.
001	WN3b	1	89	0.60	1600	0.14	-3.32	1.9	-5.18	5.30	2.6	12	0.0		
002	WN2b(h)	2	141	0.30	1600	0.13	-2.36	0.8	-5.28	5.37	1.8	13	0.0		
003	WN4b	1	79	0.60	1600	0.12	-4.36	3.0	-4.88	5.51	3.2	16	0.0		
005	WN2b	2	141	0.30	1600	0.27	-2.94	0.9	-5.22	5.45	1.7	15	0.0		
006	O3 f*+O	3	56	1.80	1600	0.08	-6.59	17.7	-5.52	6.45	0.1	94	0.2	x	4,3,5
007	WN4b	1	158	−0.10	1600	0.08	-5.02	1.1	-4.48	5.84	3.8	25	0.0		
012	O2 If*/WN5	6	50	1.70	2400	0.10	-5.19	10.6	-5.53	5.80	0.5	53	0.5	x	7
013	WN10	1	28	1.00	400	0.20	-6.34	25.3	-4.69	5.56	1.1	35	0.4		
014	WN4o(+OB)	2	67	1.15	1600	0.09	-5.17	6.4	-5.21	5.86	0.7	26	0.0	?	2,8
015	WN4b	1	89	0.50	1600	0.08	-4.44	2.6	-4.83	5.57	3.1	17	0.0		
016	WN7h	7	50	0.85	1000	0.09	-6.12	10.6	-4.64	5.80	1.8	42	0.3		
017	WN4o	1	67	0.90	1600	0.11	-4.79	5.2	-4.97	5.69	1.7	20	0.0		
018	WN3(h)	2	71	1.00	1600	0.10	-4.31	4.4	-5.24	5.63	1.1	29	0.2		
019	WN4b+O5:	2	79	0.75	1600	0.16	-5.33	6.2	-4.63	6.14	1.3	39	0.0	x[c]	2
021	WN4o(+OB)	2	67	1.30	1600	0.09	-5.76	10.6	-5.11	6.30	0.3	51	0.0	?	2,8
022	WN9h	1	32	1.10	400	0.13	-7.00	25.1	-4.85	5.75	0.5	44	0.4		
023	WN3(h)	2	71	1.00	1600	0.60	-3.98	4.0	-5.30	5.55	1.1	17	0.0		
024	WN4b	1	100	0.30	2400	0.10	-4.39	2.0	-4.53	5.54	10.1	17	0.0		
025	WN4ha	2	67	1.30	1600	0.15	-4.01	4.5	-5.67	5.55	0.5	26	0.2		
026	WN4b	1	71	0.70	1600	0.14	-4.38	4.3	-4.79	5.62	3.0	18	0.0		
027	WN5b(+B1 Ia)	2	71	1.40	1000	0.23	-8.22	29.8	-4.79	7.30	0.0	587	0.2	?	9
029	WN4b+OB	2	71	0.80	1600	0.12	-4.37	3.7	-5.03	5.50	2.3	16	0.0	x	2
030	WN6h	1	47	1.10	1000	0.07	-5.48	10.0	-5.05	5.65	1.0	34	0.3		
031	WN4b	2	75	0.70	1600	0.17	-3.81	2.7	-5.09	5.33	3.0	12	0.0	?	2
032	WN6(h)	1	47	1.10	1600	0.08	-6.14	13.9	-4.63	5.94	2.1	44	0.2	x	7,10
033	O fpe/WN9?	7	28	1.30	400	0.37	-8.48	74.8	-4.43	6.50	0.2	103	0.2		
035	WN3(h)	2	71	0.90	1600	0.11	-4.11	4.2	-5.11	5.60	1.5	24	0.1		
036	WN4b/WCE+OB	2	79	0.70	1600	0.13	-4.33	3.8	-4.88	5.71	2.0	21	0.0	?	2,11
037	WN3o	2	79	0.80	1600	0.50	-4.12	3.5	-5.07	5.65	1.5	19	0.0		
040	WN4(h)a	2	63	1.20	1600	0.15	-4.41	5.4	-5.39	5.62	0.8	29	0.2	?[c]	
041	WN4b	1	100	0.40	1300	0.12	-4.11	2.1	-4.90	5.60	2.0	18	0.0		
042	WN5b(h)(+B3 I)	2	71	1.70	1000	0.30	-9.88	66.6	-4.71	8.00	0.0	-	0.4	?[c]	2,9,12
043	WN4o+OB	2	67	1.10	1600	0.13	-4.84	6.3	-5.15	5.85	0.8	25	0.0	x	2
044	WN8ha	7	45	1.10	700	0.12	-5.59	11.3	-5.12	5.66	0.6	40	0.4		
046	WN4o	1	63	1.00	1600	0.21	-4.09	4.4	-5.23	5.44	1.7	14	0.0		
047	WN3b	2	89	0.60	1300	0.20	-3.97	2.6	-5.06	5.59	1.4	18	0.0	?[c]	
048	WN4b	1	89	0.40	1600	0.10	-4.22	2.1	-4.81	5.40	4.9	14	0.0		
049	WN4:b+O8V	2	71	1.80	2400	0.15	-5.49	9.9	-5.73	6.34	0.1	122	0.6	x	2,13
050	WN5h	14	56	1.40	1600	0.18	-4.75	7.1	-5.52	5.65	0.5	39	0.4		
051	WN3b	1	89	0.60	1600	0.02	-3.39	1.9	-5.18	5.30	2.6	12	0.0		
054	WN8ha	7	38	1.30	1000	0.50	-6.23	17.7	-4.97	5.75	0.9	34	0.2		
055	WN11h	1	28	1.40	400	0.13	-7.04	32.3	-5.13	5.77	0.2	45	0.4		
056	WN4b	1	71	0.75	1600	0.12	-4.46	4.0	-4.91	5.56	2.6	17	0.0		
057	WN4b	1	79	0.60	1600	0.10	-4.04	2.7	-4.96	5.40	3.4	14	0.0		
058	WN7h	7	47	1.15	1000	0.50	-5.35	9.9	-5.13	5.64	0.8	34	0.3		
059	WN4b+O8:	2	71	1.30	1600	0.16	-6.01	11.2	-5.07	6.45	0.2	66	0.0	?	2
060	WN4(h)a	2	63	1.40	2400	0.15	-4.82	6.5	-5.40	5.78	0.8	35	0.2		
062	WN3(h)	2	71	0.90	1600	0.12	-3.85	3.4	-5.25	5.41	1.7	19	0.1		
063	WN4ha:	2	63	1.20	1600	0.10	-4.33	5.2	-5.42	5.58	0.8	36	0.4		
064	WN4o+O9:	2	71	1.10	1600	0.26	-5.18	7.1	-5.07	6.05	0.6	34	0.0	x	2
065	WN4o	2	67	0.90	1600	0.45	-4.84	5.6	-4.92	5.75	1.7	22	0.0		
066	WN3(h)	2	89	1.00	1600	0.13	-3.73	3.3	-5.42	5.78	0.5	35	0.2		
067	WN5ha	2	47	1.30	1600	0.33	-6.11	14.3	-4.91	5.96	1.1	51	0.3	?[c]	
068	O3.5 If*/WN7	6	45	1.60	1000	0.52	-6.22	16.7	-5.46	6.00	0.2	76	0.6		
071	WN4+O8:	2	63	1.30	1600	0.38	-5.16	8.2	-5.27	5.98	0.4	31	0.0	x	2
072	WN4h+O3:	2	71	1.40	1600	0.40	-4.31	5.3	-5.71	5.80	0.2	47	0.4	?	2
073	WN5ha	14	60	1.40	1600	0.20	-4.67	6.8	-5.54	5.72	0.4	43	0.4		
074	WN3(h)a	2	79	1.25	2000	0.20	-3.82	3.7	-5.62	5.69	0.5	32	0.2		
075	WN4o	2	71	0.80	1600	0.07	-4.32	4.0	-4.99	5.56	2.2	17	0.0		
076	WN9ha	7	35	1.10	400	0.26	-6.31	17.9	-5.07	5.66	0.4	30	0.2		
077	WN7ha	7	45	1.60	1000	0.27	-5.18	41.6	-4.87	6.79	0.1	305	0.7	x[c]	7,10
078	WN6(+O8 V)	2	71	0.85	1600	0.20	-4.48	4.7	-4.96	5.70	1.7	32	0.2	?[c]	
079	WN7ha+OB	7	42	1.20	1600	0.50	-7.03	22.8	-4.46	6.17	1.9	61	0.2	?[c]	
080	WN5h:a	7	45	1.70	2400	0.50	-7.31	26.5	-4.93	6.40	0.5	87	0.2	?[c]	
081	WN5h	2	47	1.35	1000	0.33	-4.47	8.2	-5.55	5.48	0.5	32	0.4		

Table 2. continued.

BAT99	Subtype	Ref.	T_* [kK]	$\log R_t$ [$R_\odot$]	v_∞ [km/s]	E_{b-v} [mag]	M_v [mag]	R_* [$R_\odot$]	$\log \dot{M}$ [$M_\odot$/yr]	$\log L$ [$L_\odot$]	η	M^a [$M_\odot$]	X_H	Bin.[b]	Ref.
082	WN3b	1	100	0.60	1600	0.27	-3.68	1.9	-5.16	5.53	1.6	16	0.0	?[c]	
086	WN3(h)	15	71	1.00	1600	0.36	-3.37	3.1	-5.46	5.33	1.3	12	0.0		
088	WN4b/WCE	2	112	0.40	1600	0.84	-4.19	2.1	-4.81	5.80	1.9	24	0.0		
089	WN7h	1	50	0.90	1000	0.28	-5.37	10.3	-4.73	5.78	1.5	35	0.2		
091	WN6(h)	16	50	1.00	1000	0.33	-5.87	6.8	-5.15	5.42	1.3	23	0.2		
092	WN3:b(+O)+B1 Ia	7	45	1.50	1000	0.39	-8.69	50.0	-4.60	6.95	0.1	240	0.2	x[c]	7,10
093	O3 If*	6,16	45	1.80	1600	0.24	-5.65	14.9	-5.63	5.90	0.2	67	0.6	?[c]	
094	WN4b	1	141	0.00	1600	0.29	-4.80	1.3	-4.51	5.80	3.9	24	0.0		
095	WN7h+OB	16	50	0.80	1600	0.25	-6.36	13.3	-4.21	6.00	4.9	48	0.2	x	7
096	WN8	7	42	1.10	1000	0.70	-7.55	28.1	-4.37	6.35	0.9	80	0.2		
097	O3.5 If*/WN7	6,16	45	1.70	1600	0.60	-7.19	23.7	-5.18	6.30	0.3	115	0.6		
098	WN6	7	45	1.40	1600	0.80	-8.11	37.5	-4.43	6.70	0.6	226	0.6		
099	O2.5 If*/WN6	6,16	45	1.80	1600	0.30	-6.77	14.9	-5.63	5.90	0.2	42	0.2	x[c]	7
100	WN7	7	47	1.00	1000	0.28	-6.80	17.7	-4.52	6.15	1.0	59	0.2	?[c]	
102	WN6	7	45	1.30	1600	0.70	-8.38	42.1	-4.21	6.80	0.8	221	0.4	?[c]	7
103	WN5(h)+O	16	47	1.30	1600	0.40	-7.13	19.9	-4.70	6.25	0.9	87	0.4	x[c]	7,10
104	O2 If*/WN5	6	63	1.50	2400	0.38	-5.48	9.0	-5.34	6.06	0.5	66	0.4		
105	O2 If*	6	50	1.80	1600	0.30	-6.93	21.1	-5.41	6.40	0.1	134	0.6	?[c]	
106	WN5h	1	56	1.30	2400	0.35	-6.86	19.0	-4.55	6.51	1.0	130	0.4		
107	O6.5 Iafc+O6 Iaf	17	35	1.50	1000	0.26	-7.45	37.9	-4.78	6.31	0.4	95	0.4	x[c]	10,17
108	WN5h	1	56	1.40	2400	0.37	-7.10	28.8	-4.43	6.87	0.6	256	0.4		
109	WN5h	1	56	1.40	2400	0.39	-6.50	23.4	-4.56	6.69	0.7	179	0.4		
110	O2 If*	6	50	1.70	2400	0.41	-6.36	17.1	-5.22	6.22	0.4	113	0.7		
111	WN9ha	1	45	1.70	1000	0.43	-7.00	22.3	-5.42	6.25	0.1	118	0.7	?[c]	
112	WN5h	1	56	1.30	2400	0.44	-7.20	18.4	-4.57	6.48	1.0	99	0.2	?[c]	18
113	O2 If*/WN5	6,16	50	1.70	1600	0.28	-6.08	14.8	-5.49	6.09	0.2	54	0.2	x[c]	7
114	O2 If*/WN5	6,16	63	1.70	2400	0.31	-6.18	13.9	-5.35	6.44	0.2	116	0.4	?[c]	
116	WN5h:a	7	63	1.30	2400	0.75	-7.93	28.1	-4.29	7.05	0.5	390	0.4	?[c]	7
117	WN5ha	2	63	1.40	2400	0.19	-6.33	13.3	-4.93	6.40	0.5	109	0.4		
118	WN6h	1	47	1.10	1600	0.16	-7.96	31.9	-4.09	6.66	1.4	136	0.2	x[c]	7,19
119	WN6h+?	1	47	1.20	1600	0.29	-7.64	28.8	-4.31	6.57	1.0	116	0.2	x[c]	7,10
120	WN9h	1	32	1.40	500	0.15	-6.53	20.6	-5.33	5.58	0.3	32	0.3		
122	WN5h	2	50	1.15	1600	0.28	-6.90	17.3	-4.56	6.23	1.3	67	0.2		
124	WN4	2	63	1.10	1600	0.30	-4.32	4.5	-5.37	5.45	1.2	15	0.0		
126	WN4b+O8:	2	71	1.10	1600	0.22	-6.05	11.1	-4.78	6.44	0.5	65	0.0	?[c]	2
128	WN3b	2	112	0.30	1600	0.17	-3.74	1.4	-4.93	5.44	3.4	14	0.0		
129	WN3(h)a+O5 V	20	79	1.25	2000	0.35	-5.01	6.7	-5.24	6.20	0.4	64	0.2	x	7
130	WN11h	1	28	1.30	200	0.25	-6.70	29.1	-5.35	5.68	0.1	41	0.4		
131	WN4b	2	71	0.75	1600	0.13	-4.76	4.6	-4.83	5.67	2.5	20	0.0		
132	WN4b(h)	2	79	0.50	1600	0.23	-4.82	3.3	-4.67	5.58	4.4	17	0.0		
133	WN11h	1	28	1.35	200	0.11	-6.85	29.4	-5.42	5.69	0.1	41	0.4		
134	WN4b	1	79	0.60	1600	0.06	-4.24	3.0	-4.88	5.51	3.2	16	0.0		

References. (1) BAT99; (2) Foellmi et al. (2003b); (3) Niemela et al. (2001); (4) Niemela et al. (1995); (5) Koenigsberger et al. (2003); (6) Crowther & Walborn (2011); (7) Schnurr et al. (2008); (8) Breysacher (1981); (9) (Smith et al. 1996, and references therein); (10) Moffat (1989); (11) Crowther et al. (1995b); (12) Seggewiss et al. (1991); (13) Niemela (1991); (14) Crowther & Hadfield (2006); (15) Doran et al. (2013); (16) Evans et al. (2011); (17) Taylor et al. (2011); (18) Schnurr et al. (2009a); (19) Sana et al. (2013b); (20) Foellmi et al. (2006).

Notes. [(a)] Masses calculated from the luminosity, using the mass–luminosity relation derived by Gräfener et al. (2011) [(b)] x = detected, ? = questionable [(c)] high X-ray emission